JOURNAL OF AIRCRAFT
Vol. 29, No. 5, Sept.–Oct. 1992

Physics of Vortical Flows

Jean M. Délery*
Office National d'Etudes et de Recherches Aérospatiales (ONERA), 92320 Châtillon, France

Separation in three-dimensional flows leads to the formation of vortical structures resulting from rolling up of the viscous flow "sheet," initially contained in a thin boundary layer, which springs up from the surface into the outer perfect fluid flow. A clear physical understanding of this phenomenon must be based on a rational analysis of the flowfield structure using the critical-point theory. With the help of this theory, it is possible to interpret correctly the surface flow patterns that constitute the imprints of the outer flow and to give a rational and coherent description of the vortical system generated by separation. This kind of analysis is applied to separated flows forming on typical obstacles, the field of which has been thoroughly studied by means of visualizations and probings using multihole pressure probes and laser velocimetry. Thus, the skin friction line patterns of a transonic channel flow and of a multibody launcher are interpreted. Then, the vortical systems of a delta wing and an afterbody at an incidence are considered. The last two configurations are a missile fuselage-type body and an oblate ellipsoid.

I. Introduction

FLIGHT at high-incidence of combat aircraft or hypersonic vehicles during re-entry, as well as that of tactical missiles, raises practical interest on the study of three-dimensional separated flows. Applications also concern internal flows, in particular air intakes and turbomachines in which the often complex geometry of the channel and the existence of shock waves almost inevitably lead to boundary-layer separation.

In three-dimensional flows, separation entails the formation of *vortical structures*—frequently, but improperly, called *vortices* to simplify—formed by rolling up of the viscous flow "sheet," previously confined in a thin layer attached to the wall, which suddenly springs into the outer nondissipative flow. Although it has been known for a long time, this phenomenon is still incompletely understood from a physical point of view and it is delicate to model due to the flowfield complexity, all the components of which are difficult to capture properly.

Many predictive methods are based on perfect fluid models, the first of which use the vortex sheet concept. Such a sheet is defined as a surface of tangential discontinuity for the velocity field. The computational method can use different schemes: doublets, vortex filaments, vortex particles, and so forth. Publications in this domain are too numerous to be cited here. A greater accuracy in flow prediction can be obtained in the solution of the complete Euler equations, which allows, in theory, automatic capture of sheet-like discontinuities.[1–5] Perfect fluid models can give a very faithful representation of the flow past complicated geometries; however, they are unable to predict the separation process itself, which is in essence a viscous phenomenon. It is only in some special situations (e.g., the sharp leading edge or trailing edge of a wing, the flat base of a projectile) that "common sense" or the numerical viscosity of the code allows the localization of vortex sheet origins; that is, the separation lines.

When separation occurs on a regular obstacle, with a surface whose radius of curvature is large everywhere compared to the local boundary-layer thickness, the separation lines must be supplied to the perfect fluid calculation. These separation lines must be determined either by empirical correlations or by a boundary-layer calculation, possibly coupled with the external flow calculation.

In fact, a really satisfactory solution to the problem can be obtained only by solving the Navier-Stokes equations that contain the complete physics of the phenomenon. Of course, this approach raises several difficult problems in the domains of numerical methods and turbulence modeling. It also requires large computer resources. However, the results already published show that Navier-Stokes calculations allow a precise prediction of separated flows, especially in regions where separation takes place.[6–15]

Spectacular progress in the theoretical domain has been accompanied by a true breakthrough in the area of flow diagnostics. Indeed, the development of accurate exploration techniques using multihole pressure probes or laser doppler velocimetry has permitted a detailed and comprehensive definition of the structure of complex flowfields.

This article describes the separation process in three-dimensional flows and the formation of vortical structures using some of these experimental results. The purpose is to identify, or recall, some of the physical evidence, knowledge of which is prerequisite to the understanding of three-dimensional separated flows and the evaluation of numerical models.

First, the separation problem itself is considered because, this concept must be defined carefully for three-dimensional flows. In effect, going from two dimensions to three dimensions requires a total reconsideration of the separation problem with the introduction of both more general concepts and at the same time a more precise terminology.

Then, we examine the question of the vortex that progressively lifts off from the surface while increasing in intensity and size. Different kinds of vortex generation are studied by examining separation occurring on models with typical shapes. The organization of the resulting flows is established by considering, in particular, situations where several vortical structures can form.

II. Separation in Three-Dimensional Flows

For a two-dimensional steady flow, it is generally accepted that separation occurs when the skin friction τ_w goes to zero at a point S, the separation point. Downstream of S, a region exists where τ_w is negative—the velocity distribution along a normal to the obstacle surface including, near the wall, a portion where the longitudinal component u is opposite the main flow direction. The flow frequently reattaches some distance downstream of S at a point R, where the skin friction

Received March 19, 1991; revision received June 19, 1991; accepted for publication July 31, 1991.

*Head, Fundamental Aerodynamics Division. Member AIAA.

passes through zero to become positive again. As shown in Fig. 1a, the flow is organized as a recirculation bubble, often called a vortex, where the streamlines form closed curves. A special streamline, the so-called discriminating streamline, originates in the separation point S and terminates in the reattachment point R. This streamline isolates the fluid trapped in the bubble from the fluid flowing from upstream infinity to downstream infinity.

In three-dimensional flows, the definition of separation as the zero crossing of the skin friction is inadequate and, even, ineffective. In effect, on a three-dimensional obstacle, there are generally no privileged directions along which the sign of the skin friction—which is now a vector—has a well defined physical meaning. Exceptions are some very special situations such as a plane of symmetry or the case of an infinite swept wing. Furthermore, Fig. 1a no longer corresponds to reality because a three-dimensional flow has the capability to develop transverse components, allowing the fluid to escape laterally. Figure 1a must be replaced by Fig. 1b where, in the plane considered, the "streamline" stagnating at the reattachment point R is distinct from the "streamline" emanating from the separation point S. The fluid flowing between these two lines escapes in vortex T. These concepts must be clarified. In fact, two-dimensional concepts are not adequate to describe three-dimensional flows and their use, as the use of the associated terminology, are frequently a source of confusion.

Decisive advances that led to a rational and general definition of three-dimensional separation were made by the work of Legendre,[16-18] Oswatitsch,[19] and Lighthill.[20] The theoretical analyses developed by these authors can be, in particular, applied to the often complex pattern revealed by a surface flow visualization obtained by coating the obstacle surface with an oil film. Such patterns can be identified (with some precautions) with the obstacle skin friction line pattern. Visualizations of this kind are essential information for elucidating the structure of three-dimensional flows and they are widely used to detect separated zones.

A. Critical-Point Theory

The following considerations apply to a steady flow, hence, in principle to a laminar flow. In fact, it is possible to include turbulent flows in the discussion by considering a mean flow, the properties of which are defined from stationary time-averaged values; that is, values independent of time. Steady representations of this kind are fictitious but they are consistent with flow models involving the conventional Reynolds-averaging concept, hence with theoretical models using the time-averaged Navier-Stokes equations.

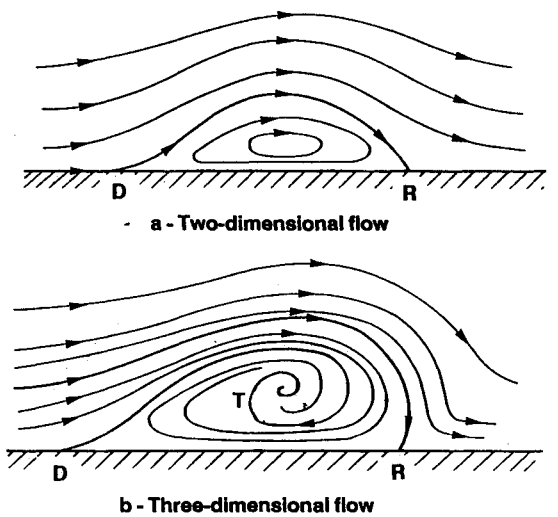

Fig. 1 Simple conceptions of separation.

As is known, when the distance y from the obstacle surface approaches zero, the direction of the velocity vector—whose modulus is zero at the wall—approaches a limit colinear with the skin friction vector τ_w. At the same time, the streamline approaches a limit position, a limiting streamline or wall streamline. Taking the aforementioned into consideration, this line is also a trajectory, or line of force, of the vector field τ_w. For this reason, it is called a skin friction line. This concept, which can be associated with a measured quantity (the skin friction), seems to be the most suitable. Consequently, it is adopted in the following developments.

The discussion of separation in three-dimensional flows is based on the critical-point theory. This theory comes from the work of Poincaré (1892) on the singular points of systems of differential equations. In its generality, it applies to a space with n dimensions. However, for the sake of simplicity, in what follows we consider the two-dimensional space constituted by the surface of an obstacle. The results for a three-dimensional flowfield are used in the description of vortical structures but without theoretical justifications.

Under these conditions, we consider an orthogonal system of coordinates (x, z) on the surface and we denote the components of the skin friction vector τ_w along x and z as $\tau_x(x, z)$ and $\tau_z(x, z)$ respectively.

For a steady flow, the skin friction lines are defined by the following autonomous (time-independent) differential system:

$$\frac{dx}{\tau_x(x, z)} = \frac{dz}{\tau_z(x, z)} \tag{1}$$

The above equations define an infinity of solution curves called characteristic lines or trajectories, which are identified here with skin friction lines. In general, one, and only one trajectory passes through a point on the surface. The only points that do not satisfy this rule are the singular points of system (1) where the skin friction vanishes; that is, where we simultaneously have

$$\tau_x(x, z) = 0, \quad \tau_z(x, z) = 0$$

To study the shape of the trajectories in the vicinity of a singular point $P_0(x, z)$, a solution is sought by a first order Taylor series expansion:

$$\tau_x(x, z) = \left(\frac{\partial \tau_x}{\partial x}\right)_{P_0}(x - x_0) + \left(\frac{\partial \tau_x}{\partial z}\right)_{P_0}(z - z_0)$$

$$\tau_z(x, z) = \left(\frac{\partial \tau_z}{\partial x}\right)_{P_0}(x - x_0) + \left(\frac{\partial \tau_z}{\partial z}\right)_{P_0}(z - z_0)$$

For convenience, in what follows the origin is placed in point P_0 and subscript 0 is omitted, hence the system

$$\frac{dx}{\frac{\partial \tau_x}{\partial x}x + \frac{\partial \tau_x}{\partial z}z} = \frac{dz}{\frac{\partial \tau_z}{\partial x}x + \frac{\partial \tau_z}{\partial z}z}$$

Assuming that the partial derivatives of τ_x and τ_z are not simultaneously equal to zero in the singular point and denoting as λ and μ two constant factors, we can write

$$\frac{dx}{\frac{\partial \tau_x}{\partial x}x + \frac{\partial \tau_x}{\partial z}z} = \frac{dz}{\frac{\partial \tau_z}{\partial x}x + \frac{\partial \tau_z}{\partial z}z} = \frac{\lambda\, dx + \mu\, dz}{\lambda\left(\frac{\partial \tau_x}{\partial x}x + \frac{\partial \tau_x}{\partial z}z\right) + \mu\left(\frac{\partial \tau_z}{\partial x}x + \frac{\partial \tau_z}{\partial z}z\right)} \tag{2}$$

A solution is sought by putting Eq. (2) in the form of a logarithmic derivative, hence

$$\frac{\mathrm{d}(\lambda x + \mu z)}{S(\lambda x + \mu z)} = \frac{\lambda\,\mathrm{d}x + \mu\,\mathrm{d}z}{\lambda\left(\frac{\partial \tau_x}{\partial x}x + \frac{\partial \tau_x}{\partial z}z\right) + \mu\left(\frac{\partial \tau_z}{\partial x}x + \frac{\partial \tau_z}{\partial z}\right)}$$

Such a form is possible if the following conditions are satisfied:

$$\left(\frac{\partial \tau_x}{\partial x} - S\right)\lambda + \frac{\partial \tau_z}{\partial x}\mu = 0$$

$$\frac{\partial \tau_x}{\partial z}\lambda + \left(\frac{\partial \tau_z}{\partial z} - S\right)\mu = 0$$

In order for this homogenous system in λ and μ to have nontrivial solutions, it is necessary for its determinant to be equal to zero; hence, the condition for S

$$\begin{vmatrix} \frac{\partial \tau_x}{\partial x} - S & \frac{\partial \tau_z}{\partial x} \\ \frac{\partial \tau_x}{\partial z} & \frac{\partial \tau_z}{\partial z} - S \end{vmatrix} = 0 \qquad (3)$$

The behavior of the skin friction lines in the vicinity of the singular—or critical—point P_0 is determined by the nature of the solutions to Eq. (3); that is, by the real or imaginary character and the sign of eigenvalues S_1 and S_2, solutions of Eq. (3).

Introducing the Jacobian matrix

$$F = \begin{vmatrix} \frac{\partial \tau_x}{\partial x} & \frac{\partial \tau_z}{\partial x} \\ \frac{\partial \tau_x}{\partial z} & \frac{\partial \tau_z}{\partial z} \end{vmatrix}$$

and letting $p = -\text{trace of } F$ and $q = \text{determinant of } F$, the eigenvalues are given by

$$S_{1,2} = \frac{-p \mp \sqrt{p^2 - 4q}}{2}$$

The different types of behaviors obtained according to the eigenvalues are situated in plane $[p, q]$ shown in Fig. 2 and the trajectories in the vicinity of the critical point are shown in Fig. 3. In the representation of Fig. 3, the canonical form is adopted, that is, the eigenvectors are perpendicular (for details, see Chanetz[21]). The canonical form, which can always be obtained by a suitable change of coordinates, corresponds in the physical world to points located in a plane of symmetry. It is to be noted that the above problem is not determined because parameters λ and μ can be arbitrarily chosen. A solution to the fluid mechanics problem would require insertion of Taylor series expansions in the Navier-Stokes equations.

If the two eigenvalues S_1 and S_2 are real and have the same sign, the singular point is a node. If they are distinct, all the trajectories, except one, have a common tangent at P_0 (see Fig. 3a). If the two eigenvalues are equal (points located on parabola II of equation $q = p^2/4$), all the trajectories have

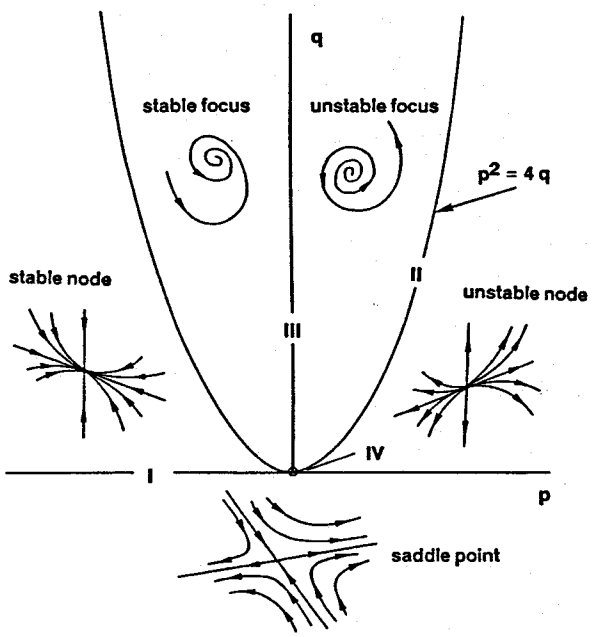

Fig. 2 Classification of critical points.

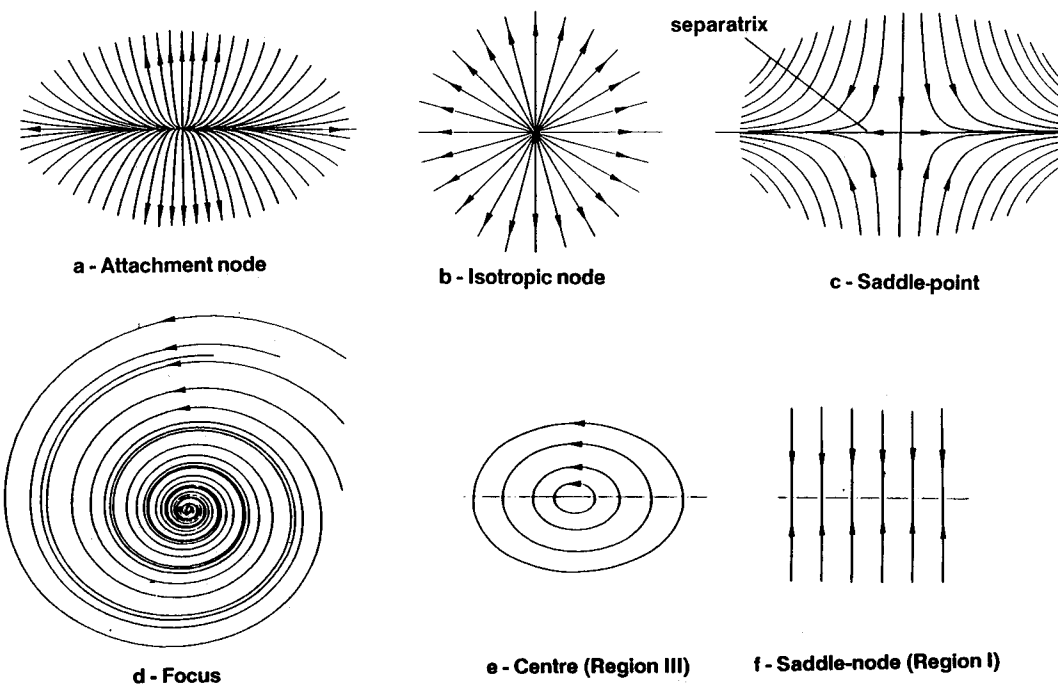

Fig. 3 Trajectories in the vicinity of a critical point.

different slopes at P_0. The node is then said to be an isotropic node (see Fig. 3b).

If the eigenvalues are real and have opposite signs (i.e., if q is negative) the singular point is a saddle point. Then, only two trajectories go through the singular point P_0, the other trajectories avoid P_0 and take on a hyperbolic shape, as shown in Fig. 3c.

If the eigenvalues are imaginary conjugate, the trajectories all end in the singular point and spiral around it to form a focus (see Fig. 3d). If p is zero for q positive (region III in Fig. 2), the singular point is not reached. Then the trajectories are closed curves having the shape of an ellipse (see Fig. 3e). This singular point is called a center.

If $q = 0$ (region I in the plane $[p, q]$), the solution has the form sketched in Fig. 3f. It can be interpreted as an infinite set of nodes and saddle points.

As shown in Fig. 2, trajectories in the vicinity of a focus or a node can be followed by moving either away from or toward the critical point. According to the theory of dynamic systems, the critical point is then said to be instable or stable. In fluid mechanics, where trajectories are interpreted as streamlines or skin friction lines the critical point is called an attachment point if the fluid flows away from it, or a separation point if the fluid flows toward it.

A similar distinction has to be made between saddle point of attachment and saddle point of separation. However, in this case the distinction that is less obvious requires an examination of the outer flow behavior in the region of the critical point, as will be seen in the following section.

As seen below, saddle points and foci are closely linked to the separation phenomenon. In fact, nodes and foci are topologically equivalent: they are sources or sinks for streamlines. Hence, it is possible to demonstrate the following relation between the number of nodes/foci and saddle points contained in the surface flow pattern of an isolated obstacle:

$$\Sigma \text{ nodes} - \Sigma \text{ saddle points} = 2 \qquad (4)$$

This relation can be useful to check the consistency of a three-dimensional flow description in terms of critical points. However one should be aware that it applies to a complete obstacle.

The two trajectories that go through a saddle point are called separators. It will be seen that they play a special, important role in the flowfield topology.

Although the critical-point theory is relatively old as concerns its application to fluid mechanics, there is renewed interest in it because of the need to have a rational framework to apprehend complex three-dimensional flows.[22-27] Furthermore, this theory is a precious tool for interpreting and analyzing the mass of results produced by modern experimental and theoretical methods applied to the study of three-dimensional flows.[28-31]

B. Separation Surface, Attachment Surface, and Vortex Sheet

The above concepts can be generalized to the streamlines of the three-dimensional flow surrounding an obstacle because they can be applied to any continuous and steady vector field. However, because the mathematical formalism is much more complicated, we give only essential results without theoretical justifications.

Also, considering the flow in a cut plane P—operation frequently used to describe three-dimensional fields—it is possible to determine the lines of force of the vector field constituted by the velocity projections in P. The set of these "pseudostreamlines" can also be interpreted in terms of critical points and separators. This is done in Fig. 1b, which represents a situation where the velocity has a component normal to the figure. However, it should be noted that such a picture of the flowfield is not objective because it depends on the chosen plane of projection P. Except in very special situations—a plane of symmetry for example—projected field lines of force are not streamlines. Thus, to avoid any confusion we will call them trajectories, or, better, lines of force that correspond to their exact definition.

A separation or attachment line is the trace on the obstacle of a stream surface of the three-dimensional flow that plays a special role. In effect, it is a barrier separating the streamlines into two families having different origins; that is, coming from different nodes.

For an obstacle, separation surfaces and/or attachment surfaces are attached to the skin friction lines emanating from a saddle point. The nature of this saddle point, which can be of the separation or the attachment type, can only be deter-

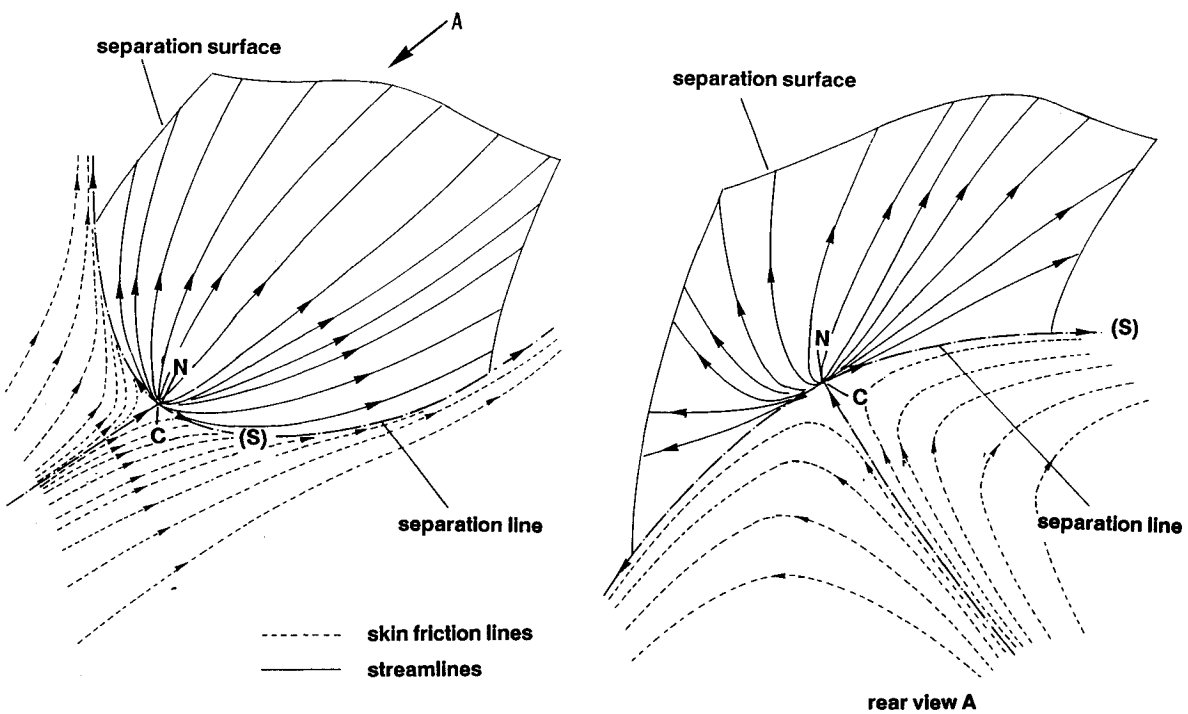

Fig. 4 Flow structure in the vicinity of a saddle point of separation.

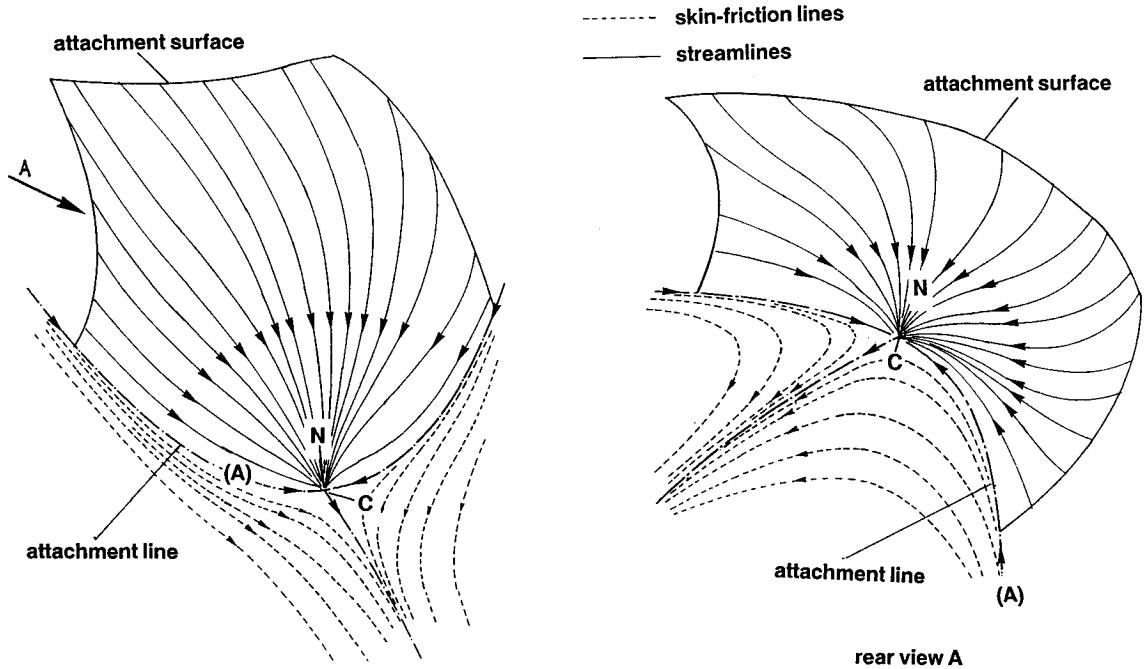

Fig. 5 Flow structure in the vicinity of a saddle point of attachment.

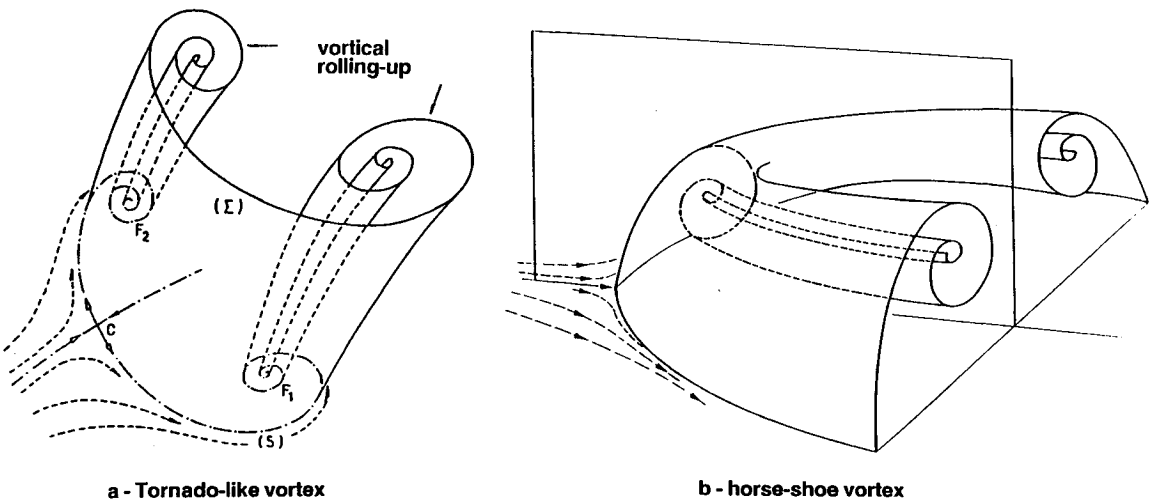

Fig. 6 Separation surface and formation of vortices.

mined by examining the behavior of the outer flow in the vicinity of the critical point. The need to consider the entire three-dimensional field in order to define the flow physics unambiguously was pointed out by Legendre[32] and emphasized by Chapman.[33]

To make this point clear, Fig. 4 shows a schematic representation of the flow in the vicinity of a saddle point of separation. In this situation, the streamlines constituting what is called the separation surface Σ emanate from a node N—more precisely a half node—coincident with saddle point C. The streamlines of Σ flow away from N, the trace of Σ on the obstacle being the skin friction line—constituting the separation line S—emanating from the saddle point.

The situation at a saddle point of attachment is shown in Fig. 5. Now, what is called the attachment surface Σ is constituted by the outer flow streamlines flowing in the direction of the node N coincident with C. In an attachment process, the attachment surface Σ passes through the skin friction lines, defining an attachment line A, going into the saddle point C. The existence of a stream surface such as Σ intersecting the obstacle is possible because of the special nature of S or A.

In the case of separation, the separation surface Σ can be assimilated to what is called a separation or vortex sheet, although the concept of sheet—defined as a surface of tangential discontinuity for the velocity field—pertains to a perfect fluid model of the separated flow. In reality, for a viscous flow, the velocity and vorticity fields are continuous so that it is frequently difficult to define such sheets from inspection of the experimental results.

Due to its origin, the separation surface is located in a region of the field where the vorticity tends to concentrate and the vortical structures (typical of separated three-dimensional flows) can be interpreted as a rolling up of the separation surface. Most often, a separation line S ends at a focus around which it spirals. This focus is the trace on the obstacle of the vortex resulting from the rolling up of the separation surface sustained by S. Such a situation, with two foci F_1 and F_2 on either side of throat C, is depicted in Fig. 6a. It corresponds to what is called a tornado-like vortex. The focus "sustaining" the vortex can be in a plane of symmetry, as seen in the examples below: this case corresponds to a horseshoe vortex (see Fig. 6b).

Because of the rolling up of the separation surface, the vorticity generated in the boundary layer that migrated into the outer flow tends to concentrate in the core of the structure. Thus, far from the wall, the field consists of isolated regions

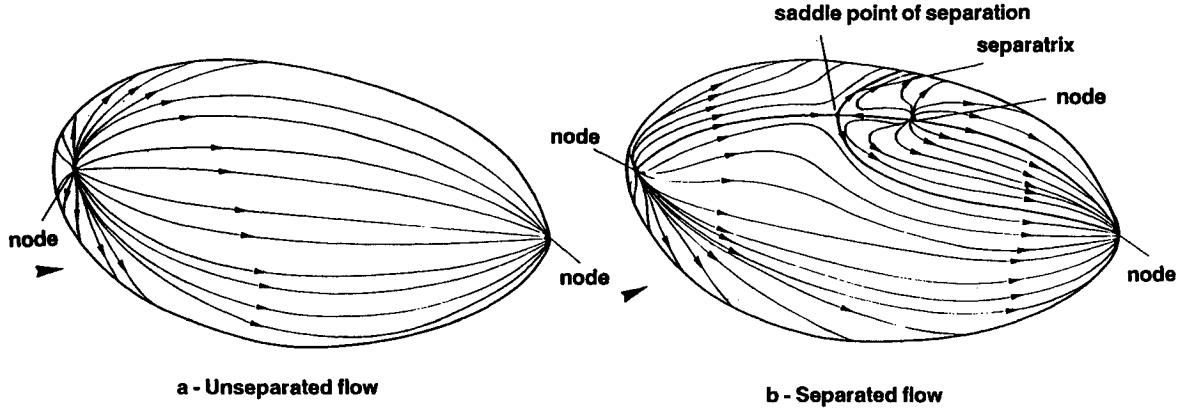

Fig. 7 Separation on a three-dimensional obstacle.

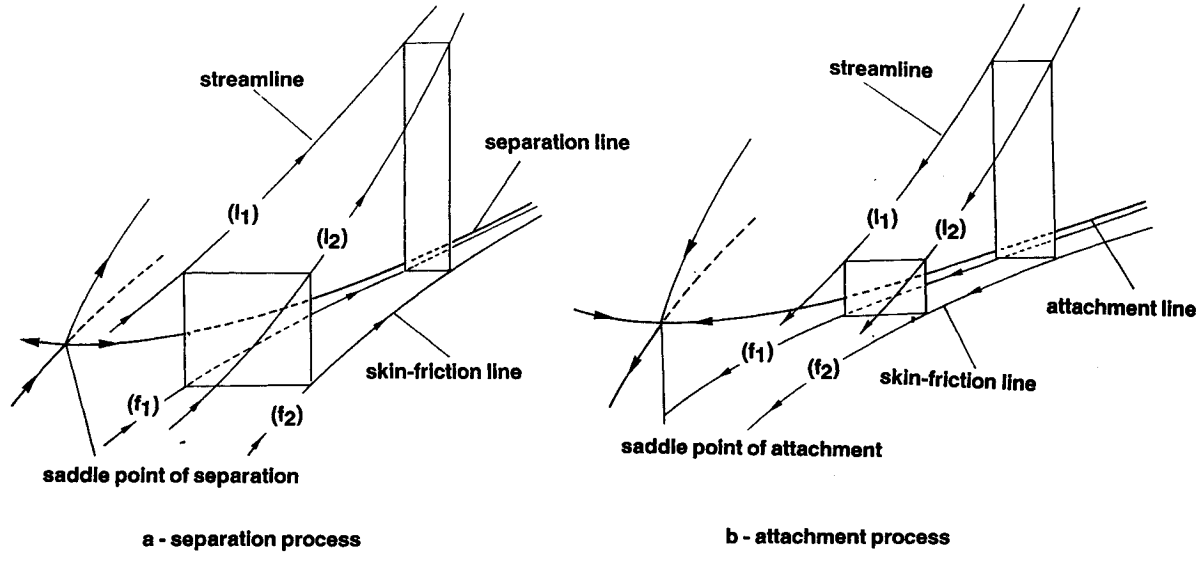

Fig. 8 Flow in the vicinity of a separation or reattachment line.

where the vorticity is concentrated. This well-known property is utilized by perfect fluid models. It can also be used to describe a separated flow by consideration of a "vortex skeleton."[34,35]

C. Separation and Attachment on an Obstacle

The simplest situation that can be conceived is an elongated, regular body at zero or very low incidence. In this case, the surface flow pattern comprises an attachment node at the front stagnation point and a separation node located on the rear part of the body. All the skin friction lines covering the obstacle originate in the attachment node; they all terminate in the separation node, as shown in Fig. 7a.

As a consequence of an increase of the angle of incidence, for example, the surface flow pattern may contain more than two nodes. Because the skin friction lines passing through two nodes of the same nature cannot intersect, a critical point, necessarily of the saddle type, must be located somewhere between these two nodes (see Fig. 7b). It will be concluded that the flow is separated if its surface flow pattern contains—at least—one saddle point that is of the separation type (see section B). Through this saddle point go two special skin friction lines—the separators—one of them being the separation line. Such a line defines two domains in the surface flow. The skin friction lines belonging to each of these domains have different origins; that is, come from different nodes.

The skin friction lines of each of these two families flow parallel to the separation line so that it is frequently impossible to determine the line of the surface pattern that is the separation line, which is not distinct from the other skin friction lines, except that it originates in a saddle point. However, under the action of an adverse pressure gradient, the skin friction lines close to the separation line tend to converge toward the separation line, which now becomes well distinct from the other skin friction lines. This phenomenon may occur far downstream of the saddle point that is the origin of the separation line. As shown by Lighthill,[20] using very simple arguments, this convergence of the skin friction lines has deep repercussions on the external flow structure.

Indeed, referring to Fig. 8a let us consider an infinitely small stream tube with a rectangular cross section, bounded by two streamlines l_1 and l_2 and two skin friction lines f_1 and f_2. The mass flow crossing section nh of this stream tube is given by

$$q_m = \rho n h \bar{V}$$

where $\bar{V}$ is an average value of the velocity assumed to remain parallel to the wall and to vary linearly over distance h locally normal to the wall. Furthermore, it is assumed that in a separation process, the velocity close to the separation line decreases when the distance from the saddle point of separation increases. Then we have

$$h = (q_m/\rho n \bar{V})$$

This relation shows that convergence of the skin friction lines toward a separation line $n \to 0$ leads to an increase in h. In other words, the streamlines closest to the obstacle tend to leave the surface in the vicinity of a separation line. The result is a strong thickening of the dissipative regions.

The faster the skin friction lines converge, the more rapidly the streamlines "take off." This motion can lead (as the ex-

perimental results presented below show) to a surging in the outer nondissipative flow of the viscous part of the flow initially contained in a thin boundary layer. This phenomenon is certainly the most typical and the most spectacular feature of separation in three-dimensional flows.

The local behavior of the skin friction lines in the vicinity of a separation line S has been the subject of many discussions, because surface flow visualizations often lack sufficient resolution to show what really occurs. According to the original interpretation of Maskell,[36] there is a contact between S and the neighboring skin friction lines, the separation line being in this case a locus of cusp points. This interpretation was contested by Legendre[17] and by Lighthill,[20] who argued that such a concentration of singularities was highly improbable. In fact, the convergence of the skin friction lines toward the separation line—when it occurs—is without contact at finite distance.

In other words, what can be called effective separation, defined as a phenomenon characterized by a rapid thickening of the dissipative regions until they invade the perfect fluid flow, must be associated not with the occurrence of a separation line but with the rapid convergence motion of the skin friction lines. As already mentioned, this convergence can occur relatively far from the saddle point, which is, strictly speaking, the real cause of separation. This distinction, in fact purely quantitative and not concerning the essence of the separation phenomenon, is at the origin of many controversies, in particular those concerning the concepts of open or closed separation (Wang[23]). In fact, open separation does not exist; a separation is always closed in the sense that, by definition, separation implies the existence of a separator that "closes" or isolates one domain in the flowfield.

To summarize:

1) We can say that separation occurs if a separator exists in the skin friction line pattern. Existence of such a line is necessarily linked to the presence of a saddle point, which must be of the separation type.

2) Effective separation takes place when the skin friction lines converge toward a separation line.

The symmetrical attachment process can be defined, mutatis mutandis, in identical terms, with the difference that now the skin friction lines diverge from the separator, which becomes an attachment line. In this situation, the velocity along the attachment line tends to increase with increasing distance from the saddle point, so that the distance h separating the outer flow streamlines from the surface in the region of the attachment surface now can decrease.[37,38] Thus, in this case, the outer flow "dives" toward the wall (see Fig. 8a).

The notion of separator is applied to true separation as well as to attachment (or reattachment). Hence, the term separation line is sometimes used with the generic meaning of separator without making a distinction between the physical concepts of separation and attachment. This lack of rigor in language leads to a certain confusion tending to obscure the concept of separation in three-dimensional flows even more. To avoid this difficulty, in what follows a clear distinction is made between separator, separation line, and attachment line, although these concepts are identical from a mathematical point of view.

D. Case of the Two-Dimensional Separated Flow

Two-dimensional separation—planar or axisymmetric—appears as a very special case of the general three-dimensional definition. Indeed, within the framework of the preceding analysis, a two-dimensional separation (or attachment) line consists of an infinite set of saddle points located on a straight line perpendicular to the plane containing the flow (region I of the diagram represented in Fig. 2). One intuitively realizes that such a situation is highly improbable from a physical standpoint. In fact, experimental studies of nominally two-dimensional separated flows show that the (unavoidable) side effects due to the limited span of the test setup always lead to a three-dimensional situation. Even when special precautions are taken to minimize these effects, one observes that the surface flow tends to organize itself into a more or less regular three-dimensional pattern.[39,40] In axisymmetric configurations—in principle, free of side effects—the flow also has a three-dimensional structure. In particular, surface flow visualizations clearly reveal the existence at reattachment of a fine pattern in which the reattachment line is a succession of nodes and saddle points.[41] Thus, Fig. 9a shows the visualization of turbulent reattachment on a flare at Mach 5.[42] The interpretative sketch in Fig. 9b shows that the reattachment line is the locus of a finite number of nodes and saddle points, which denotes the presence of structures similar to the Görtler vortices in the flow.[43]

III. Analysis of Typical Vortical Structures

The concepts of critical points, separators, and separation surfaces apply to any continuous, steady vector field. They are not linked to a three-dimensional separation theory with a predictive capability. In fact, these concepts constitute a "grammar" allowing a rational description of complex flows by means of a rigorous and well-defined terminology.[44] Their use rapidly appears indispensable for interpreting flow visualizations or field measurements in order to obtain a consistent representation of these data.[45]

Thus, these concepts are widely used in the following sections where we describe vortical flows observed during experiments conducted, for the most part, at ONERA. The adopted presentation consists of first demonstrating the interest of the critical-point theory to interpret particularly complex wall patterns. These patterns are the imprints on the obstacle of the outer flow and a correct interpretation of the information they contain is a prerequisite to physical understanding of the flow. Then, separation phenomena occurring on different bodies are examined by successively considering the case where separation is imposed by a singular line; the case where the origin of the separation line is fixed, and the case where separation is entirely "free."

A. Wall Patterns Induced by Multiple Separations

1. *Transonic Channel Flow*

The first case is a three-dimensional channel, whose geometry is shown in Fig. 10. A bump is mounted on the channel lower wall, whose three other faces are flat. The bump line of crest is swept at an angle of 30 deg relative to the upstream velocity. The test section span is 0.120 m and its height, in the entrance section, is 0.100 m. The flow, subsonic at the channel entrance, accelerates in the converging part of the test section to reach sonic state in the vicinity of the bump summit that constitutes a throat. Downstream, the flow becomes supersonic; then, because of the choking effect of an adjustable second throat, it decelerates through shock waves, which interact strongly with the turbulent boundary layers developing on the four channel walls.

The main objective of this experiment was to produce, with a simple geometry, a highly three-dimensional flow as a test case to validate computational methods.[46] Thus, this flow was thoroughly investigated by means of surface visualizations, pressure measurements, and field probings with a three-component LDV system.[47] In what follows, we focus our attention on surface flow visualizations in order to illustrate the interest of the critical-point theory to describe a particularly complex flow.

The interpretative sketches in Fig. 11 were made from the photographs of the surface flow visualizations and from direct observation of these visualizations during the test, which revealed information that was lost when the picture was taken. Although these sketches are meant to be only of qualitative value, they do remain within the proportions of reality.

Examining the flow over the bump (Fig. 11a), we can see that two foci, F_1 and F_2, exist and are clearly visible in the

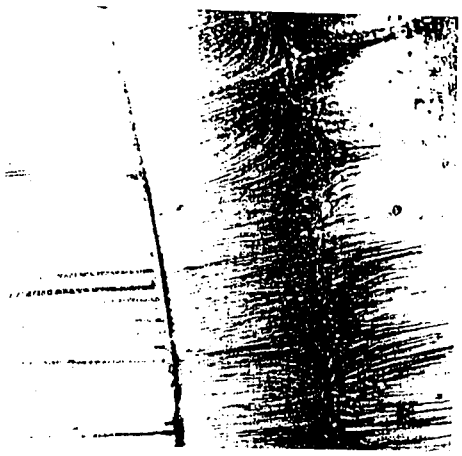

a - Surface flow visualization

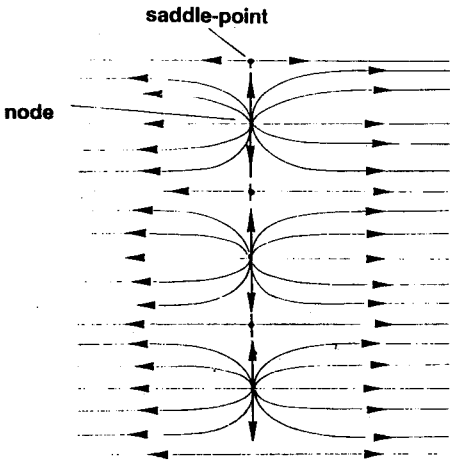

b - Topological interpretation

Fig. 9 Reattachment of an axisymmetrical flow.

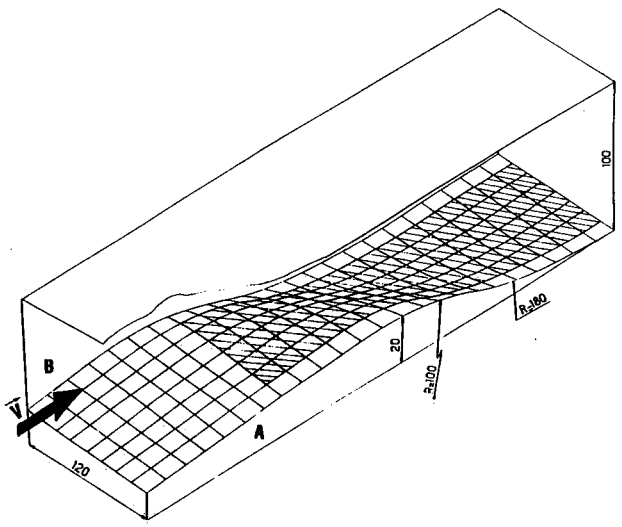

Fig. 10 Definition of the three-dimensional transonic channel.

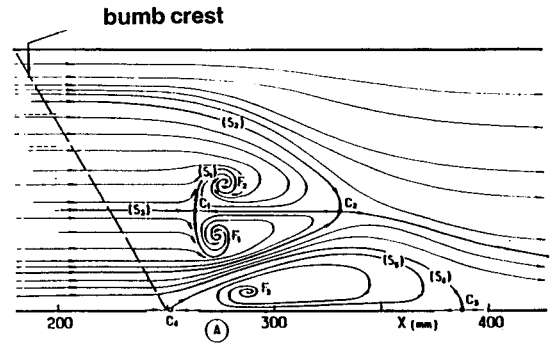

a - Face bearing the bump

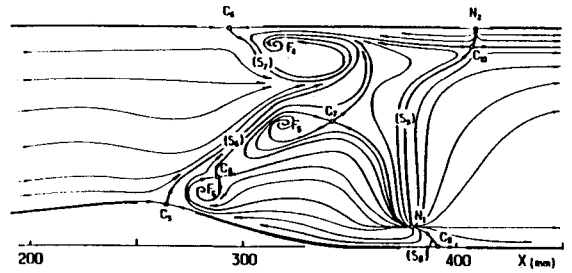

b - Sidewall A

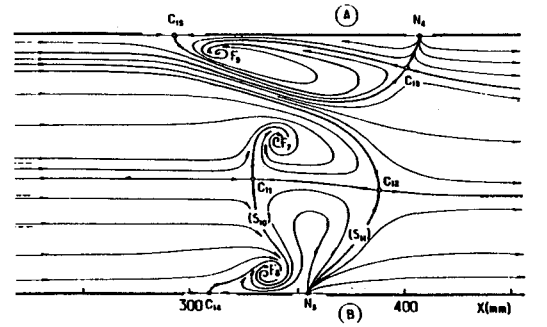

c - Top wall

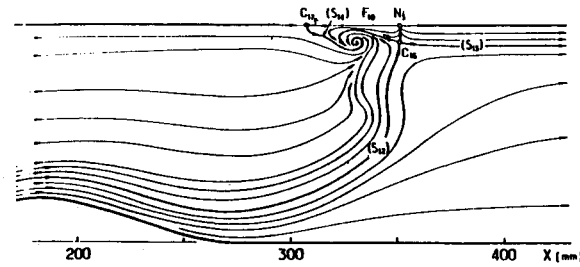

d - Sidewall B

Fig. 11 Three-dimensional transonic channel; topological interpretation of surface flow patterns.

left half of the channel. The separator S_1 passing through saddle point C_1 and spiralling around F_1 and F_2 constitutes a "barrier" approximately at the root of the oblique shock of the lambda shock system attached to the interaction.

The skin friction lines from upstream and contained in the domain delimited by the separator S_2 passing through saddle point C_2 wind around either F_1 or F_2, according to their locations on one side or the other of the separator S_3, which carries both C_1 and C_2. One set of these lines goes around the barrier S_1 by abruptly curving backward. The structure, including S_1, S_2, and the two foci F_1 and F_2, is conventionally observed in shock-wave/boundary-layer interactions in a channel with three-dimensional effects.[48–50]

In such a situation, S_1 can be associated unambiguously with a well-characterized separation and S_2 with an attachment. Thus, C_1 and C_2 are, respectively, a separation and an attachment saddle point. The spirals winding around foci F_1 and F_2 are the traces on the wall of vortices escaping in the outer flow, with separation line S_1 being the origin of a separation surface that winds around the axes of the vortical structures, in conformity with the sketch of Fig. 9a.

Returning to the sketch in Fig. 11a, we observe that the skin friction lines from upstream divide into two families. The

first, near face B, all flow continuously downstream. The others, near wall A, separate in turn into two subfamilies 1) the lines included between S_2 and separator S_4—an attachment line—leading to half-saddle point C_3, that continue their path downstream; and 2) the lines between wall A and S_4 that wind around a third focus F_3 to form a "vortex," delimited by the separator S_5—a separation line—from half-saddle point C_4.

A similar description can be made for the patterns observed on the other walls of the channel. But, let us simply note the complexity of the pattern on wall A where a node N_1 and a half-node N_2, located at the junction with the channel upper wall, are the origins of the skin friction lines of the surface flow downstream part, those from upstream disappearing in focus F_4.

Cumulating the corresponding half-nodes and half-saddle points, and remembering that a focus is topologically equivalent to a node, the count of all the singular points leads to the relation

$$\Sigma \text{ nodes} - \Sigma \text{ saddle points} = 15 - 13 = 2$$

where, in the count of nodes, we have added two fictitious nodes at upstream and downstream infinity, which are the source and the sink of the skin friction lines, respectively.

Very thorough discussions of this kind applied to similar flows have identified pattern modifications occurring when one parameter is varied; for example, the Reynolds number or the Mach number.[30,31,51] Indeed, experiments show that, in the case of the channel flow considered here, slight changes in the test conditions can lead to dramatic changes in the location and number of critical points.

2. *Space Launcher First Stage*

In some particularly complex situations, the establishment of a topologically consistent surface pattern requires information on the outer flow structure. Indeed, oil flow visualizations frequently have insufficient fineness to reveal all the wall flow critical points and separators. In this case, a correct flow definition is achieved by matching the outer field and the surface flow.

To illustrate this point, let us consider the example provided by a study of the flow past a 0.01-scale model of the future European space launcher ARIANE 5 afterbody. As shown in Fig. 12, these experiments were conducted on a centerbody-type arrangement. The incoming flow Mach number was equal to four and the jets of the two lateral boosters and of the central engine were simulated by high-pressure air. In addition to surface flow visualizations, the field was probed by an LDV system, which allowed the definition of the flow organization in the internozzle region.[52]

A schlieren photograph showing the jets from the boosters and the central engine is reproduced in Fig. 13. Due to the simulated altitude (30 km), these jets expand largely and interact strongly with one another downstream of the nozzle exit planes, causing an intense backflow in the direction of

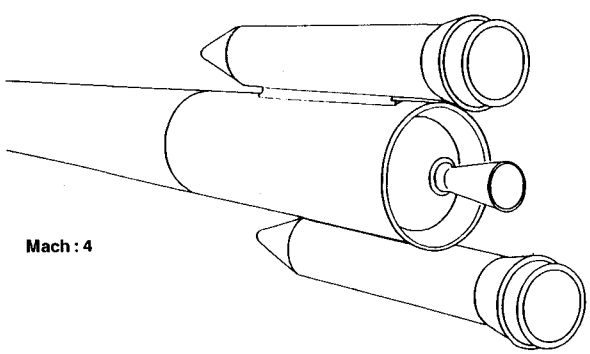

Fig. 12 Afterbody of the future European space launcher ARIANE 5.

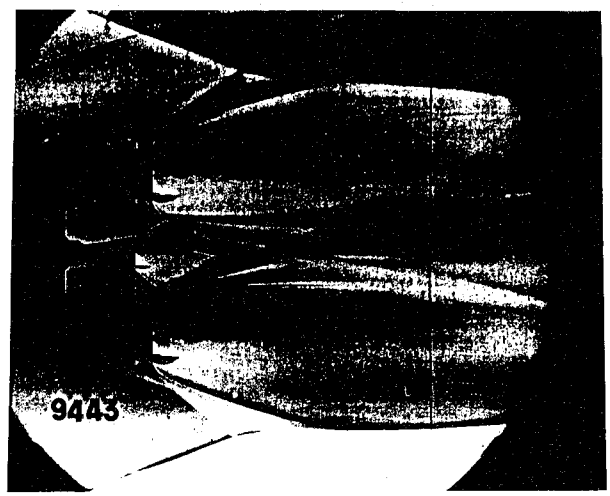

Fig. 13 ARIANE 5 afterbody; schlieren picture of jets; upstream Mach number $M_\infty = 4$.

the central engine base. Furthermore, jet pluming may induce outer flow separation upstream of the booster and/or central engine bases. An interpretation of the observed surface flow pattern is presented in Fig. 14.

First, considering the central engine, we can see a separator S_1—a separation line—from saddle point C_1 located upstream of the assembly part attaching the booster to the central engine. Line S_1 first runs toward the plane of symmetry perpendicular to the figure, coming very close to the separator A_1—an attachment line—contained in this plane. Then, it gradually leaves A_1 and, close to the base, S_1 suddenly bends to point toward separation node N_2, practically following the base edge. Downstream of C_1, an attachment node N_1 exists at the base of the assembly part and is the origin of a family of skin friction lines f_1. Thus, separator S_1 separates family f_1 from family f_2 including skin friction lines from upstream, originating in a node type singular point located outside the visualized domain.

A second separation line S_2 originates in saddle point C_2. It separates family f_1 from family f_3 of skin friction lines originating in node N_3. The three families f_1, f_2, and f_3 end up at separation node N_2. The description of this part of the flow must be completed by introduction of the separation line S_3 passing through saddle point C_3 and coincident with the base edge.

The main separation linked to S_1 is certainly induced by impact on the central body of the shock wave forming ahead of the booster nose. However, the separation occurring along S_2 probably results from the perturbation emanating from the end of the assembly part. It may also be due to jet pluming.

Let us now consider what occurs on the booster. An attachment node N_4—of the isotropic type—must exist on the ogive nose. Visualizations clearly show the separator S_4 coming from saddle point C_4 located near the ogive shoulder, as well as the separator S_5 from saddle point C_5 located at the base of the assembly part. The separation whose trace is S_4 may result from the reflection on the central engine of the shock wave forming ahead of the booster. One also can see attachment nodes N_5 and N_6 clearly. All the booster skin friction lines end in separation node N_7 located on the base edge. The flow organization in this region is similar to that observed on the central engine. In Fig. 14 is also represented the wall pattern on the booster side opposite the central engine. This view makes the converging motion of all the skin friction lines toward node N_7 visible.

It is not possible to apply relation (4) to this example, because only part of the obstacle is accessible to visualizations; in particular the base regions are not visible.

As previously mentioned, the consistency of such a pattern is ensured by examining the outer flowfield organization at

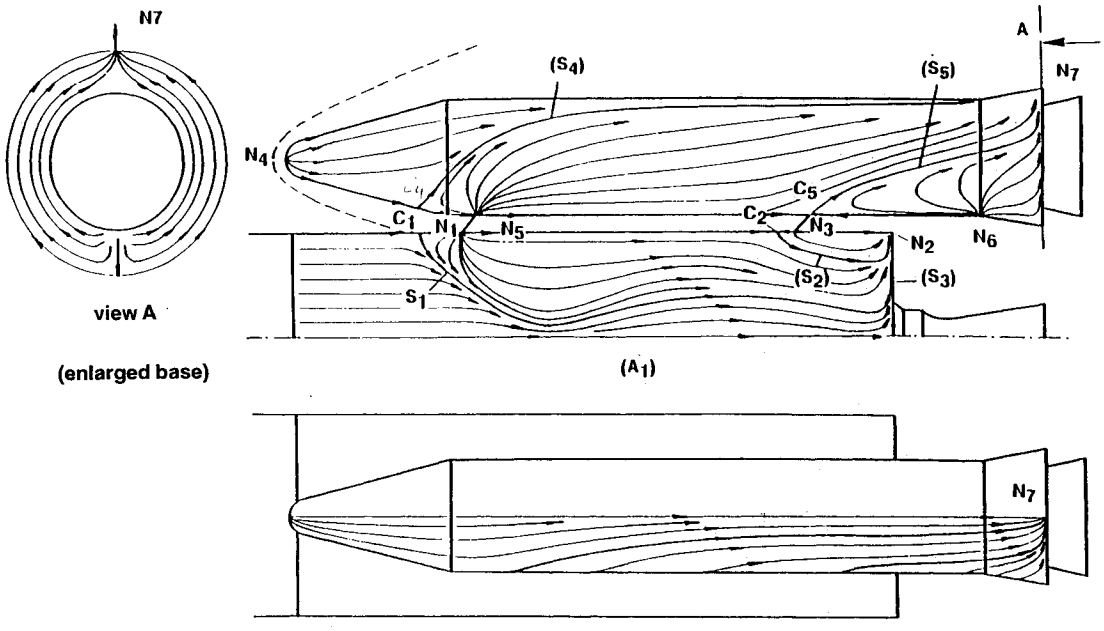

Fig. 14 ARIANE 5 afterbody; topological interpretation of the surface flow pattern; upstream Mach number $M_\infty = 4$.

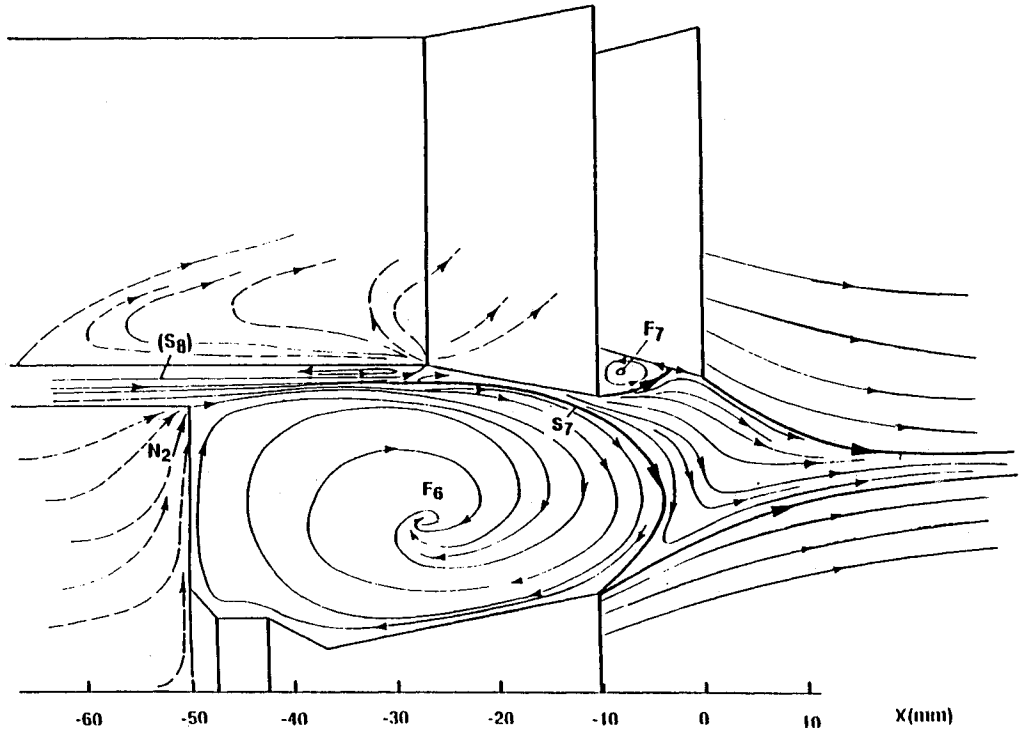

Fig. 15 ARIANE 5 afterbody; flowfield structure in a symmetry plane; upstream Mach number $M_\infty = 4$.

the same time. Let us consider Fig. 15 in which the flow streamlines in the internozzle zone plane of symmetry containing the nozzle axes are plotted. This plot shows a first focus F_6 around which wind the streamlines "trapped" in the recirculating flow. These streamlines belong to a family delimited by the separator $\mathcal{S}_7$ from upstream and ending at the nozzle lip. Thus, the streamlines flowing between the central body and $\mathcal{S}_4$ disappear into F_6. One of the streamlines winding around F_6 has its origin at the base, at a point coincident with surface flow node N_2. As seen above, there is an attachment node N_8 at the booster flare origin where a separator $\mathcal{S}_8$ ends up. The streamlines located (in the sketch) above $\mathcal{S}_8$ flow back in the upstream direction and those between $\mathcal{S}_7$ and $\mathcal{S}_8$ flow in the downstream direction. Some of these streamlines bend to flow around the recirculating flow, then abruptly turn in the downstream direction under the entrainment effect induced by the central engine jet.

B. Separation with Imposed Separation Line

1. Delta Wing with Sharp Leading Edge

For a long time, the delta wing with a sharp leading edge at an incidence has raised the interest of scientists because of the "strength" of the vortices forming above the wing suction side (which makes them easy to detect) and also because of its conceptually simple character, at first sight. Indeed, in this case, intuitive reasoning, guided by experimental observations, allows the separation line that is the origin of the sheet, whose rolling up will constitute the main vortical structure, to be fixed along the leading edge. Thus, part of the problem

has an immediate solution. Hence, this configuration is amenable to simplified analyses and very instructive theoretical results were obtained by the use of analytical methods (Legendre[16]) very early, well before the advent of supercomputers. We do not intend to review the many studies devoted to the delta wing here. Simply, let us point out that, although information on surface flow properties abounds, field measurements allowing a precise definition of the vortical structures have appeared only recently.[53–58]

Delta wing vortices form a very large family if one considers wing sweep angle, leading-edge shape, upstream flow Mach number, Reynolds number, and so forth. In what follows we restrict ourselves to description of the incompressible flow forming over a sharp leading edge wing with a 75 deg sweep angle. For this, we will utilize recent results including field probings by five-hole pressure probes and LDV.[59–61]

Under these conditions, the existence of intense suction side vortices is well demonstrated by flowfield visualizations. A surface flow visualization obtained for an incidence α = 7.5 deg and an upstream speed V_∞ = 40 m/s is shown in Fig. 16a. Due to the size of the wing (chord length C = 1.45 m, hence Reynolds number: Re_c = 4 10^6) the boundary layer is turbulent over the major part of the wing suction side. It appears clearly that the skin friction lines are parallel to the wing chord in the central part of the wing. Then, toward the leading edge, a first separator A_1—having the character of an attachment line—is visible. Closer to the leading edge, the surface flow pattern reveals a second separator. S_2—cor-

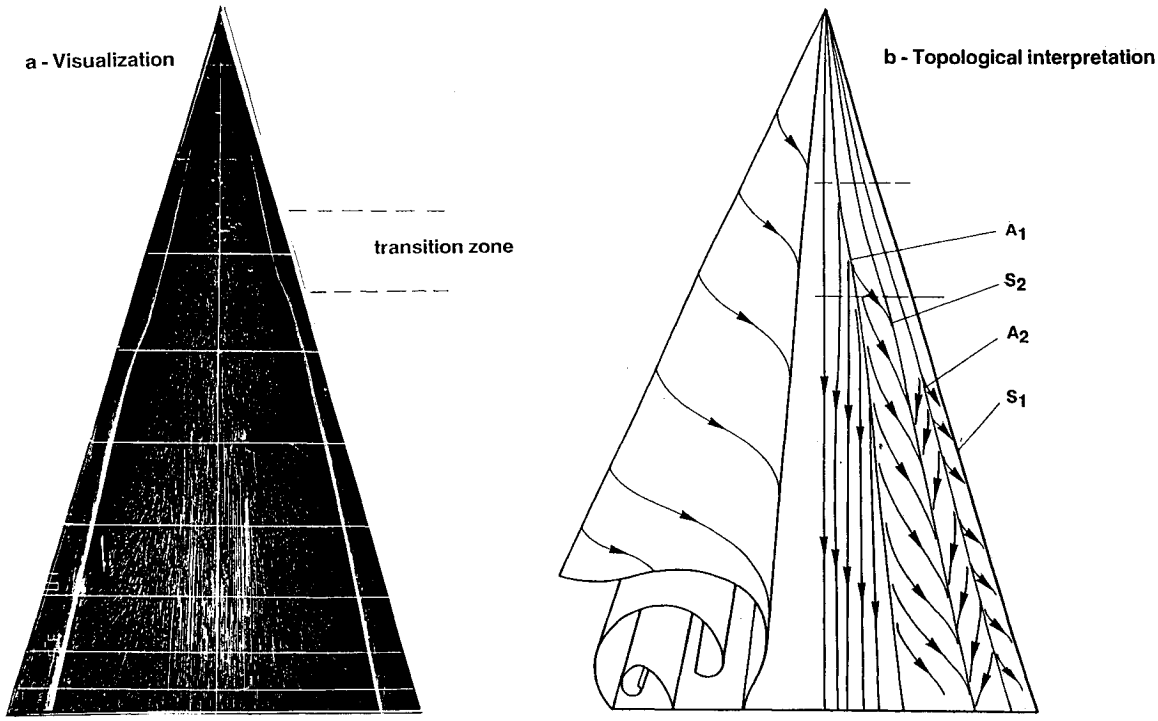

Fig. 16 Delta wing with sharp leading edge; surface flow pattern at an incidence α = 7.5 deg; upstream velocity V_∞ = 40 m/s.

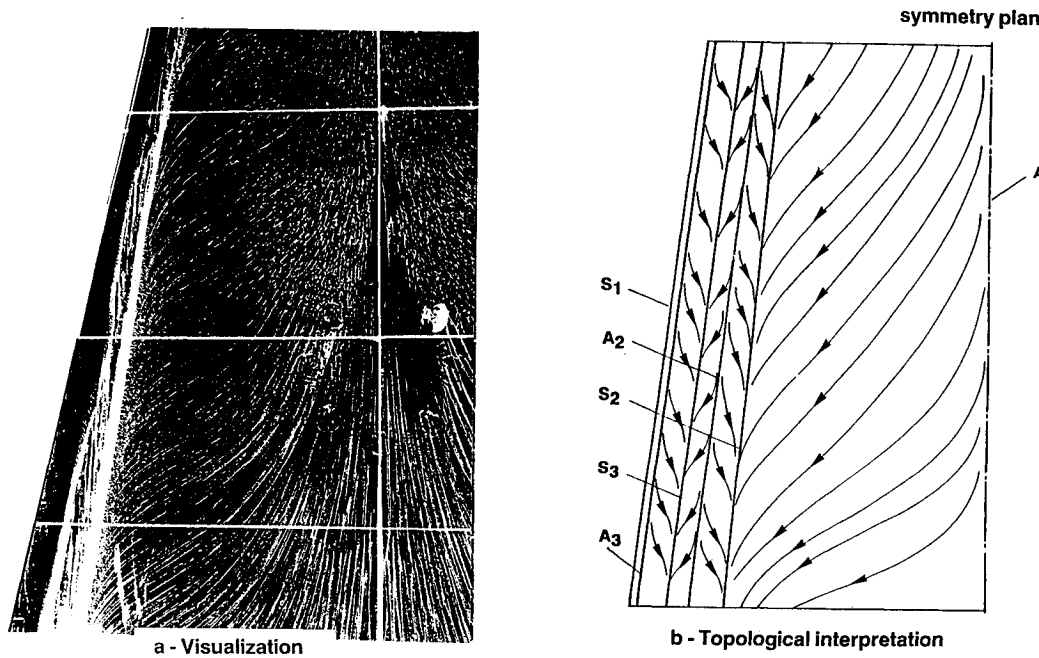

Fig. 17 Delta wing with sharp leading edge; surface flow pattern at an incidence α = 20 deg; upstream velocity V_∞ = 40 m/s.

responding to what is called secondary separation—the primary separation line S_1 being coincident with the leading edge. Figure 16b shows an interpretative sketch of this pattern, as well as of the vortex system of which it is the trace. The inflection of the separators visible shortly after the wing apex is due to boundary-layer transition.

Figure 17 shows the pattern observed when $\alpha = 20$ deg, with the field studied covering only the rear left-hand part of the wing to make details more apparent. Now three separation lines S_1—along the leading edge—S_2, and S_3 are present and the "primary" attachment line A_1 is located in the plane of symmetry. A careful examination of the visualizations allows detection of attachment lines A_2 and A_3, which must exist between the separation lines.

It should be noted that the organization of this type of flow is relatively insensitive to the Reynolds number when the angle of incidence is high. Hence, it is possible to complete the above description by examining results obtained at $V_\infty = 20$ m/s with a smaller model (chord length $C = 0.5$ m, Reynolds number: $Re_c = 0.7\ 10^6$), for which detailed field measurements were made. Thus, Fig. 18a shows the velocity field projected in a vertical plane located at the reduced abscissa $X/C = 0.58$, the incidence being equal to 20 deg. A trajectography in this plane, with consideration of the surface flow pattern, was used to draw the sketch in Fig. 18b, which shows the existence of the following critical points on the wing: 1) half-saddle point $\mathscr{C}_1$, $\mathscr{C}_2$, and $\mathscr{C}_3$ corresponding to separation lines S_1, S_2, and S_3; 2) half-saddle points $\mathscr{C}_4$, $\mathscr{C}_5$, and $\mathscr{C}_6$ corresponding to attachment lines A_1, A_2, and A_3.

Outside the wing, one observes 1) a first separator $\mathscr{S}_1$, from the half-saddle point $\mathscr{C}_1$ located on the leading edge, which winds around focus $\mathscr{F}_1$ constituting the primary vortex center; 2) a second separator $\mathscr{S}_2$ ending at attachment half-saddle point $\mathscr{C}_4$; 3) a third separator $\mathscr{S}_3$ originating at $\mathscr{C}_2$ and winding around focus $\mathscr{F}_2$, center of the secondary vortex; 4) a fourth separator $\mathscr{S}_4$ ending at half-saddle point $\mathscr{C}_5$; 5) a fifth separator $\mathscr{S}_5$ winding around focus $\mathscr{F}_3$, center of a "tertiary" vortex; and 6) last, separator $\mathscr{S}_6$ "stagnating" at critical point $\mathscr{C}_7$ located in the wing symmetry plane. The spatial organization of the different separation surfaces is depicted in Fig. 19.

The definition of the vortical field above this wing is completed by the representation in vertical planes of the quantities deduced from explorations. Thus, Fig. 20 shows distributions in three planes of Ω_x, which is the X-wise component of the rotational vector. This component measures the "strength" of the swirling motion. Such plots reveal the vortical structure mode of formation by rolling up of the sheet emanating from the leading edge in which the vorticity initially contained in the boundary layer of the upper and lower surfaces has been transferred. Also, these plots show the concentration of vorticity in the center of what will constitute the primary vortex, by far the most intense. The secondary vortex manifests itself by the presence of a region of opposite sign and much lower vorticity. The tertiary vortex is practically indistinguishable.

It should be noted that only the separation giving rise to the primary vortex is fixed by the leading-edge singularity. The other vortical structures, whose influence on the wall pressure distribution is noticeable, originate on the flat wing upper surface. Hence, they cannot be represented by perfect fluid models. Last, although experimental results already useful for validating numerical codes are available for subsonic and supersonic flows; field explorations are nearly nonexistent in hypersonic flows.[62]

2. *Base Flow*

The second example of a configuration where the main separation is fixed by a surface discontinuity is provided by an afterbody with a flat base. In this case, the flow streaming along the afterbody separates at the base edge, which gives

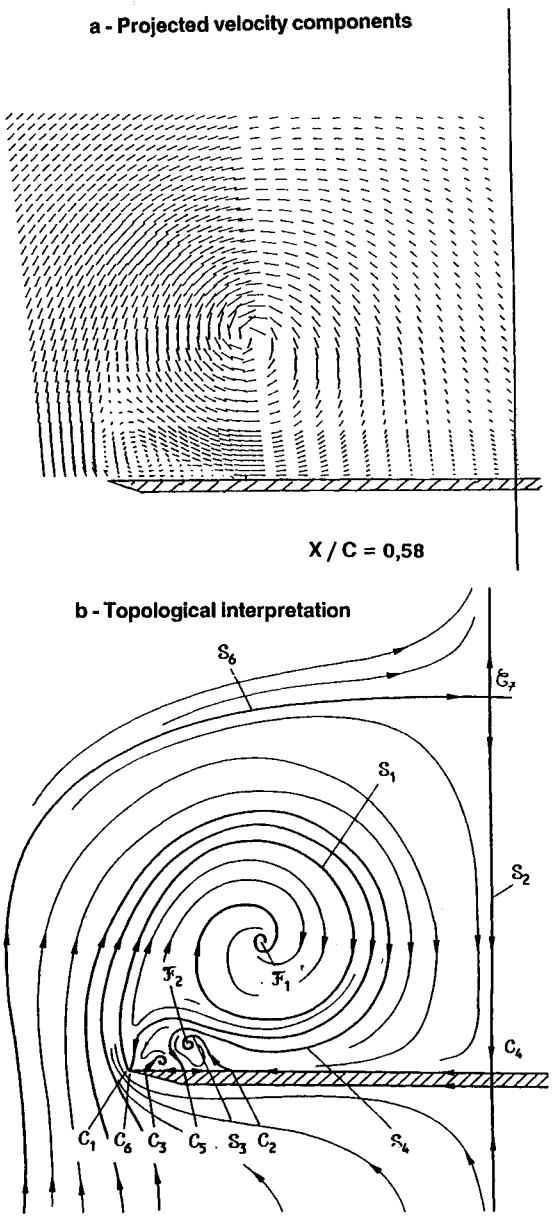

Fig. 18 Delta wing with sharp leading edge; transverse flowfield at an incidence $\alpha = 20$ deg; upstream velocity $V_\infty = 20$ m/s.

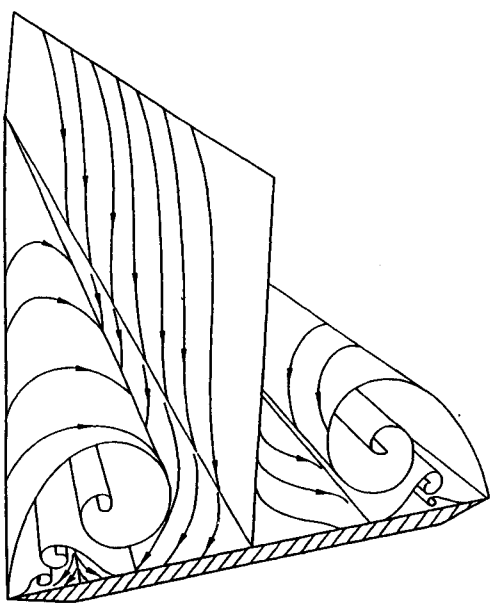

Fig. 19 Delta wing with sharp leading edge; flowfield general structure at an incidence $\alpha = 20$ deg.

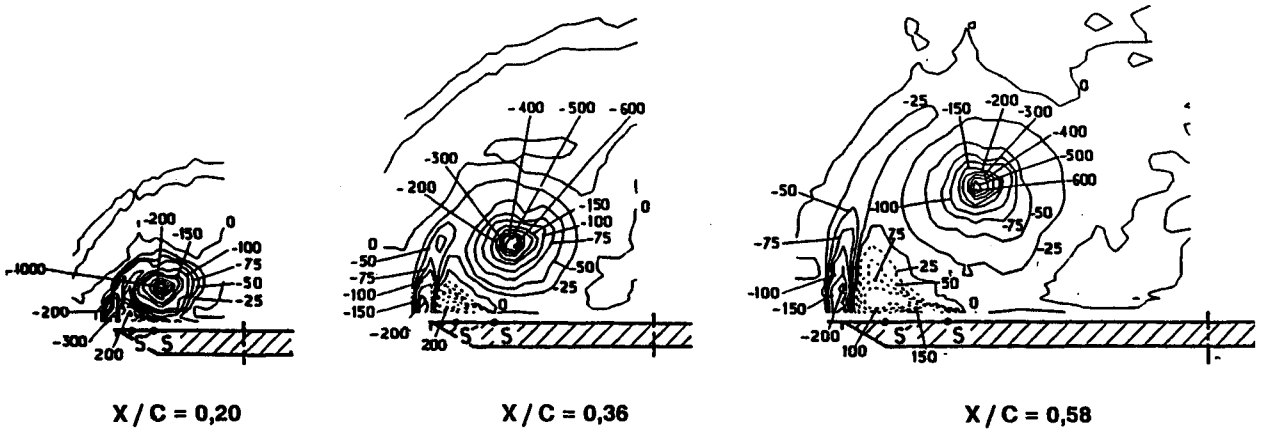

Fig. 20 Delta wing with sharp leading edge; longitudinal component of vorticity in transverse planes; angle of incidence α = 20 deg; upstream velocity V_∞ = 20 m/s.

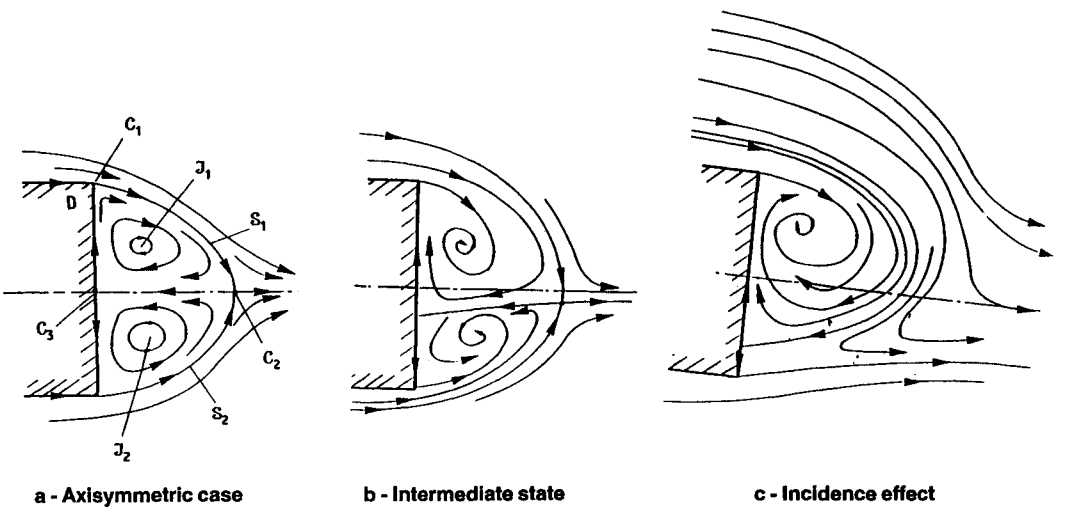

Fig. 21 Flow behind the base of an axisymmetric afterbody.

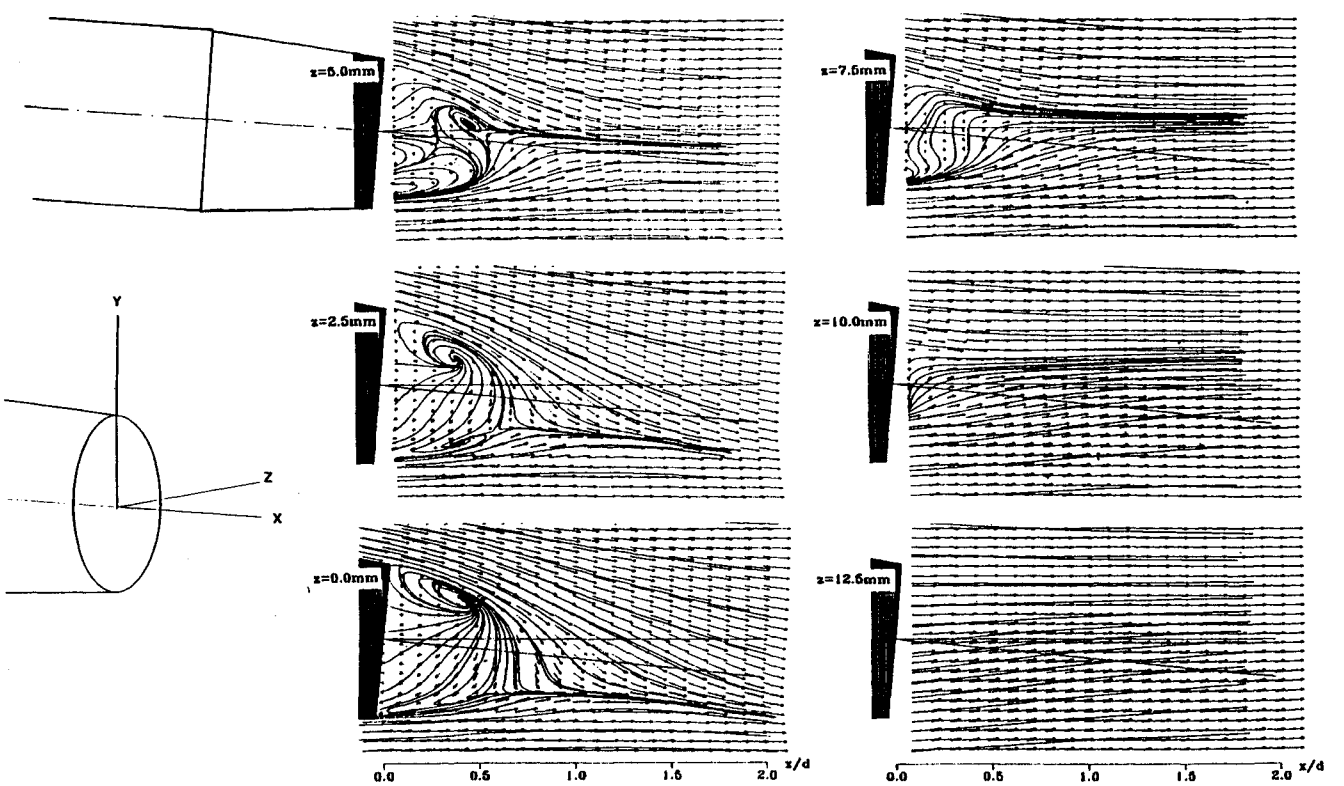

Fig. 22 Axisymmetric afterbody at an incidence α = 5 deg; upstream Mach number M_∞ = 0.54; longitudinal velocity field.[65]

rise to the formation of a large dissipative region or wake. We consider here an unpowered axisymmetric afterbody, with axis OX, the base of which is plane and perpendicular to OX. At zero incidence, the wake structure is well known (in particular, see Délery and Lacau[63]). As shown in Fig. 21a, in this case a recirculation zone organized into a toroidal vortex forms just downstream of the base. The topology in a meridian plane includes 1) a half-saddle point $\mathscr{C}_1$ at the base edge D; 2) a saddle point $\mathscr{C}_2$ inside the flow, on the centerline (the so-called reattachment point); and 3) a second half-saddle point $\mathscr{C}_3$ at the base center. The separator $\mathscr{S}_1$ joining $\mathscr{C}_1$ and $\mathscr{C}_2$ acts as a discriminating line (see Sec. II above). The line $\mathscr{S}_2$ linking the stagnation points $\mathscr{C}_1$ and $\mathscr{C}_3$ is also a separator. Inside each vortex of the meridian plane, the streamlines are closed curves turning around centers $\mathscr{F}_1$ and $\mathscr{F}_2$.

When a three-dimensional effect is introduced, the wake structure is less well known. The description that follows is relative to the flow produced when an axisymmetric afterbody is set at an incidence of 5 deg. The afterbody has a caliber $D = 0.030$ m and a 6 deg boat-tail of length $L = D$. The incoming flow Mach number is equal to 0.54, the Reynolds number computed with D being $Re_D = 3.56\ 10^5$. This configuration, which is the simplest three-dimensional situation starting from the axisymmetric case, has been investigated in great detail by means of very carefully conducted and extremely fine explorations executed with a three-component LDV system.[64,65]

It should be noted that this configuration has a plane of symmetry defined by the model axis and the velocity vector at upstream infinity. Figure 22 shows fields of the mean velocity component in four streamwise planes located at different distances Z from the vertical plane of symmetry ($Z = 0$). This representation gives a good idea of the region close to the base also called the near-wake region. As shown in Fig. 23, the flow organization in the far-wake region is more clearly revealed by fields of the mean velocity component in planes perpendicular to axis OX. To give a better understanding of the flow, the lines of force of these fields are superimposed on the vector plots of Figs. 22 and 23.

Figure 24 gives a topological interpretation of the transverse field valid for planes located at some distance from the base. This field includes a saddle point $\mathscr{C}_1$ through which passes the separator $\mathscr{S}_1$ separating the lines of force from downstream to upstream infinity from those that disappear into foci $\mathscr{F}_1$ and $\mathscr{F}_2$. A second separator $\mathscr{S}_2$, going through saddle point $\mathscr{C}_2$ acts as a barrier between the ascending and descending lines of force belonging to the region where foci form.

Now, let us examine the flow in the near-wake plane of symmetry in which the lines of force are streamlines. As indicated in Fig. 25, separator $\mathscr{S}_1$ from edge A winds around focus $\mathscr{F}_1$ and a second separator $\mathscr{S}_2$ ends at the separation point, or half-saddle point, $\mathscr{C}_2$ located on the base. Last, a third separator $\mathscr{S}_3$, originating in saddle point $\mathscr{C}_3$ coincident with lower edge B, separates the flows coming from the afterbody "leeward" and "windward" sides.

There is great difference between Figs. 21a and 21c, in which there has been a change from a topology with four saddle points and two foci to a topology with three saddle points and only one focus. The bifurcation from a to c is probably preceded, for very small angles of incidence, by situation b where centers $\mathscr{F}_1$ and $\mathscr{F}_2$ have been replaced by foci $\mathscr{F}_1$ and $\mathscr{F}_2$.

Due to the absence of surface flow visualizations, the wall patterns presented in Fig. 26 are in great part conjectural. On the body (see Fig. 26a), the pattern comprises two critical points; namely, a half-node N_1 located at the base upper edge A and a half-saddle point C_1 in the symmetrical position B. All the afterbody skin friction lines are "swallowed" by sep-

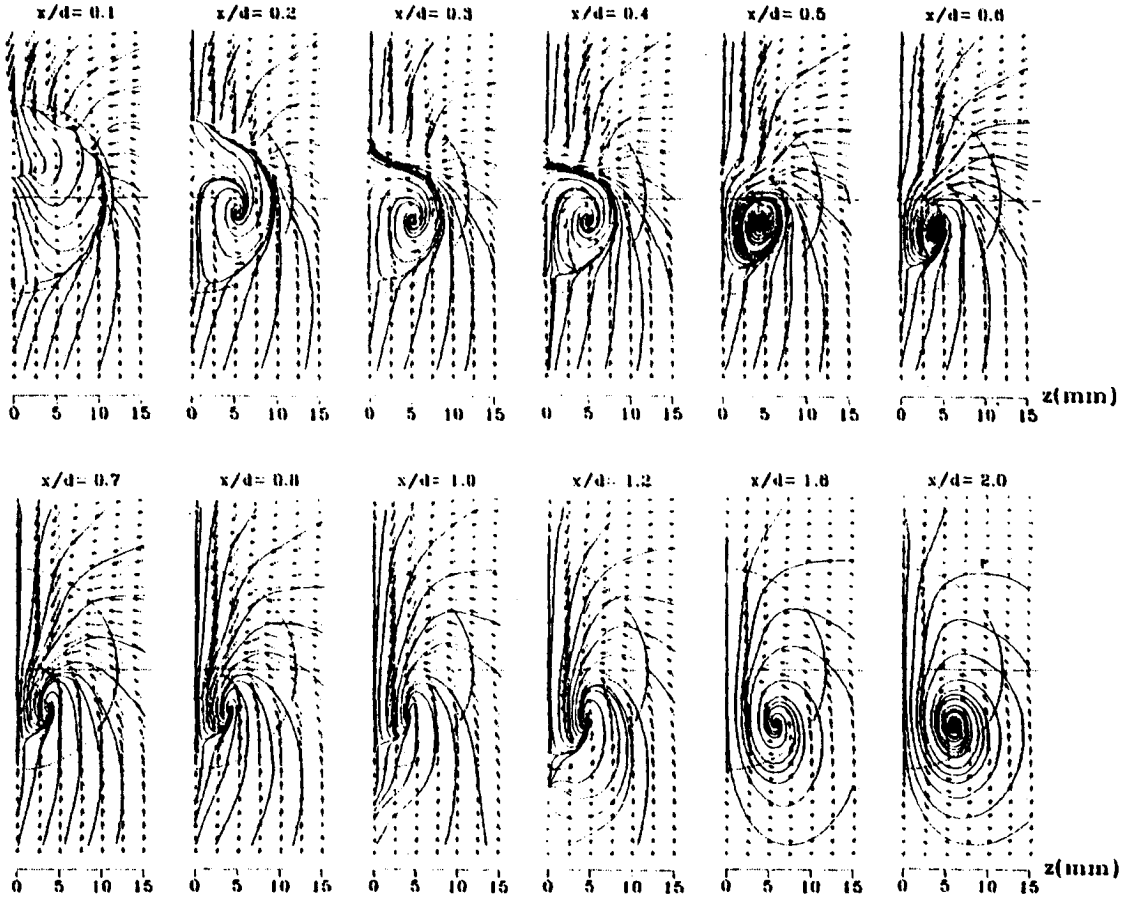

Fig. 23 Axisymmetric afterbody at an incidence $\alpha = 5$ deg; upstream Mach number $M_\infty = 0.54$; transverse velocity field.[65]

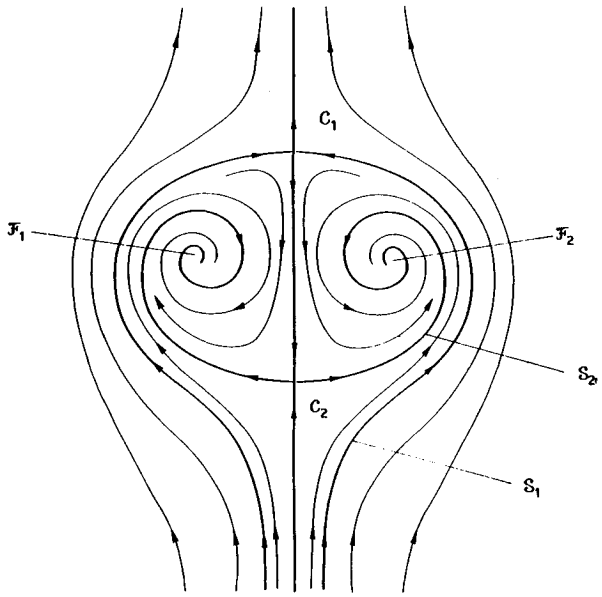

Fig. 24 Axisymmetric afterbody at an incidence $\alpha = 5$ deg; topology of the transverse flowfield in the far wake region.

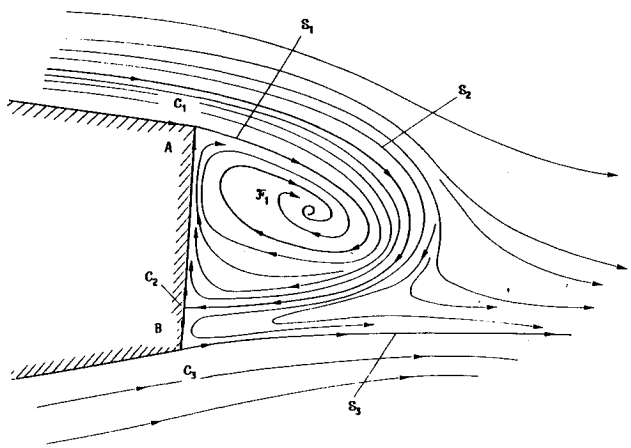

Fig. 25 Axisymmetric afterbody at an incidence $\alpha = 5$ deg; topology of the longitudinal flowfield in the near wake region.

aration node N_1. The situation on the base is shown in Fig. 26e. At B is half-saddle point C_2 (complementary of C_1) and at A half-node N_2 (complementary of N_1). Node N_3 on the base coincides with the impact point of separator $\mathcal{S}_2$: it feeds the surface flow that disappears into node N_2. Within the framework of this description, a separator S_1 runs along the base edge between saddle point $C_1 + C_2$ and node $N_1 + N_2$. Figure 26c shows the pattern in the purely axisymmetric case (no incidence). Now, an isotropic node is placed in the center of the base, whose edge carries an infinite set of saddle points. One intuitively understands that such a "special" situation is very unlikely to occur in the physical world, which explains the impossibility of experimentally achieving perfectly axisymmetric flows.

The data above were used to make the drawing in Fig. 27 representing the separation surface sustained by the separation line S_1 coincident with the base edge. In a rather complex motion, this surface rolls up to form a hem distorted into two branches bending in the downstream direction. Cutting this surface by a transverse plane gives the two foci represented in Fig. 24. This vortical structure is a horseshoe-like vortex, similar to the vortex forming ahead of a blunt obstacle.

C. Slender Body with Sharp Nose

The configuration considered here is a sharp-nosed, slender obstacle set at an incidence angle α. This geometry corresponds to a missile body or to the front part of a supersonic aircraft fuselage. In this case, the location of separation lines cannot be "guessed" in advance, but it seems obvious that

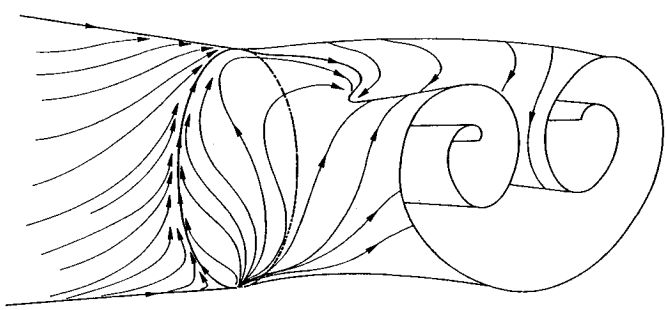

Fig. 27 Axisymmetric afterbody at an incidence $\alpha = 5$ deg; main separation surface.

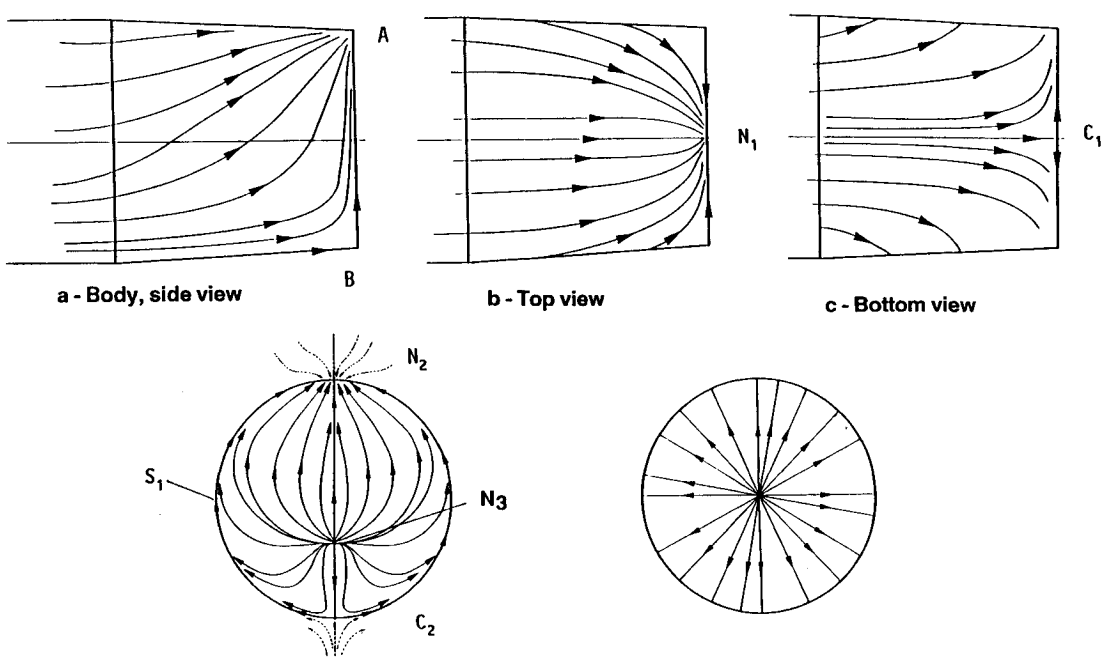

Fig. 26 Axisymmetric afterbody at an incidence $\alpha = 5$ deg; surface flow pattern.

these lines must originate on the sharp nose. Due to its great practical interest, this shape has been the subject of a large number of experimental studies, most of them consisting of wall pressure and force measurements. However, detailed studies including investigations of the vortex system generated by this kind of body are relatively scarce[66–71] (for a topological study from laser sheet visualizations, see Ref. 12).

Here, we analyze the results obtained with an axisymmetric model consisting of a cylindrical body with diameter D = 0.030 m, and a three-caliber circular ogive. Experiments were conducted in a supersonic flow of Mach number $M_\infty = 2$ and for a stagnation pressure equal to 5 10^4 Pa, which gives a Reynolds number $Re_D = 1.61\ 10^5$. Under these conditions, the boundary layer is laminar before separation.

The flow was studied for incidences in the range 5–20 deg. In each case, the surface flow pattern was carefully defined by means of oil film visualizations; the wall pressure distribution was measured; and the field was probed in several planes perpendicular to the model axis OX using a five-hole pressure probe.[72] In what follows, we consider only results obtained for $\alpha = 20$ deg. For this moderate angle of incidence, and considering the supersonic value of the flow Mach number, there was no risk of formation of an unsymmetrical vortex system.

Visualizations obtained for $\alpha = 20$ deg are presented in Fig. 28, where the starting of the separators from the ogive apex is clearly visible. As shown by the interpretative sketches, it is possible to identify four separation lines (the only ones represented) and five attachment lines. For more clarity, the surface pattern is developed in Fig. 29 by approximately preserving longitudinal and circumferential distances. The attachment line A_1 located in the windward plane of symmetry is in the middle of the drawing and the leeward attachment line A_2, divided in two, is on the sides. Separation lines S_2 and S_3 are shown in the figure, but the line located very near S_2 (called S_4 in Fig. 28) is omitted for the sake of clarity. In effect, the vortex generated by the separation taking place along S_4 is too weak to affect the transverse flow noticeably.

In this case, the vortex system clearly is detached from the surface, which allows construction of a quantitative representation of the field through flow probings. Thus, Fig. 30a shows the mean velocity field projected in the transverse plane located at the reduced abscissa $X/D = 8$, where the large primary vortex attached to separator S_1 appears very distinctly. By contrast, due to the smallness of the field, the structures generated by the other separations are barely visible. Nevertheless, by means of trajectography in this vector field and by taking the surface pattern into consideration, it was possible to make the drawing of Fig. 30b, wherein proportions of reality are respected.

The plot of the local stagnation pressure distribution also gives a vivid picture of the vortex system. Thus, Fig. 31 shows a perspective view of such distributions in planes normal to the model axis. These plots clearly reveal the regions of high vorticity—in the main vortex core and in the region of the secondary vortices—marked by a pronounced deficit in stagnation pressure. The increase with X of the vortical domain, due to a continuous surging of the boundary layers, is evident from these plots.

D. Blunt-Nosed Obstacle

Now we consider a situation where separation takes place on a blunt-nosed body whose radius of curvature is large everywhere compared to the local boundary-layer thickness. This kind of flow is even more difficult to compute because the location, as well as the origin of the separation line(s), can be determined only by an accurate prediction of the boundary-layer behavior during its evolution toward separation.

Most experiments conducted with a view to contributing to the physical understanding of this type of separation have considered bodies with an ellipsoid shape. After the first investigations by Eichelbrenner and Oudard,[73] many studies

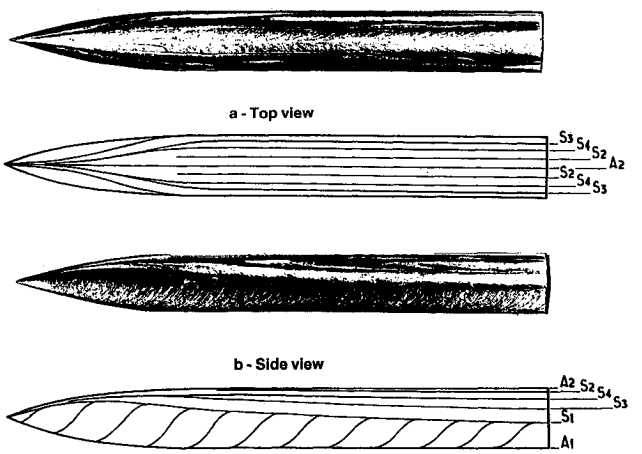

Fig. 28 Slender body with sharp nose; surface flow pattern at an incidence $\alpha = 20$ deg; upstream Mach number $M_\infty = 2$.

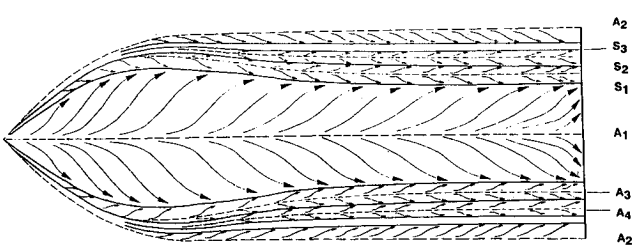

Fig. 29 Slender body with sharp nose; developed surface flow pattern at an incidence $\alpha = 20$ deg; upstream Mach number $M_\infty = 2$.

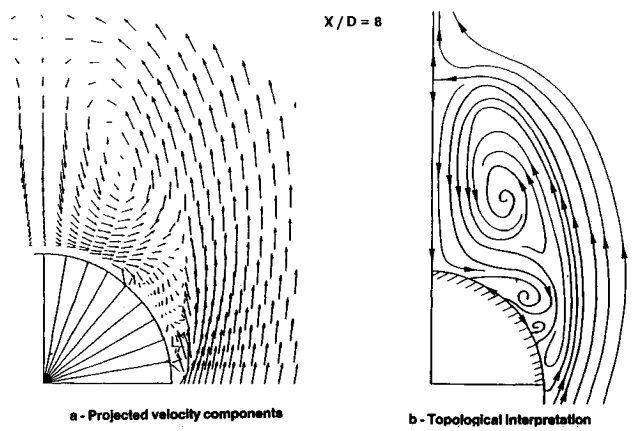

Fig. 30 Slender body with sharp nose; transverse flowfield at an incidence $\alpha = 20$ deg; upstream Mach number $M_\infty = 2$.

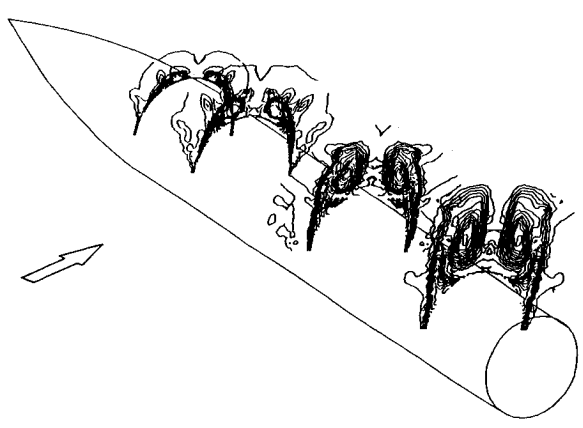

Fig. 31 Slender body with sharp nose; stagnation pressure in four transverse planes; incidence $\alpha = 20$ deg; upstream Mach number $M_\infty = 2$.

followed, most often restricted to wall pressure measurements and surface flow visualizations. Only recently quantitative information on the outer flow structure has become available.[74-77]

We consider here a study conducted on a large model consisting of a half oblate ellipsoid extended by a cylinder and terminated by a flat base. This model, with a total length L = 1.83 m, was tested at an upstream velocity V_∞ = 50 m/s for angles of incidence ranging from 0 to 30 deg. The Reynolds number being Re_L = 6.4 10^6, transition occurs in the nose region. Hence, the boundary layer is turbulent in the zone where the vortices are fully developed.[21,78,79]

Figures 32a and 32b give an interpretation of the surface patterns observed for α = 20 and 30 deg, with clear separation occurring for these values of the angle of incidence. In these diagrams, the real proportions are retained for the top and side views, while the pattern on the windward side is illustrated by means of a pseudodevelopment of this part of the model and is, therefore, approximate, although it conforms to reality.

If we ignore the base region, the pattern observed for α = 20 deg includes three separators in Fig. 32a: 1) two attachment lines A_1 and A_2, located on the leeward and windward sides, respectively, in the flow plane of symmetry; and 2) one separation line S_1 clearly visible on the rear half of the model near its lateral edges.

To have a consistent topological construction of such a pattern, at least three singular points must be introduced in the nose region of the obstacle. These are an attachment node N_1, saddle point C_1, through which pass the separation line

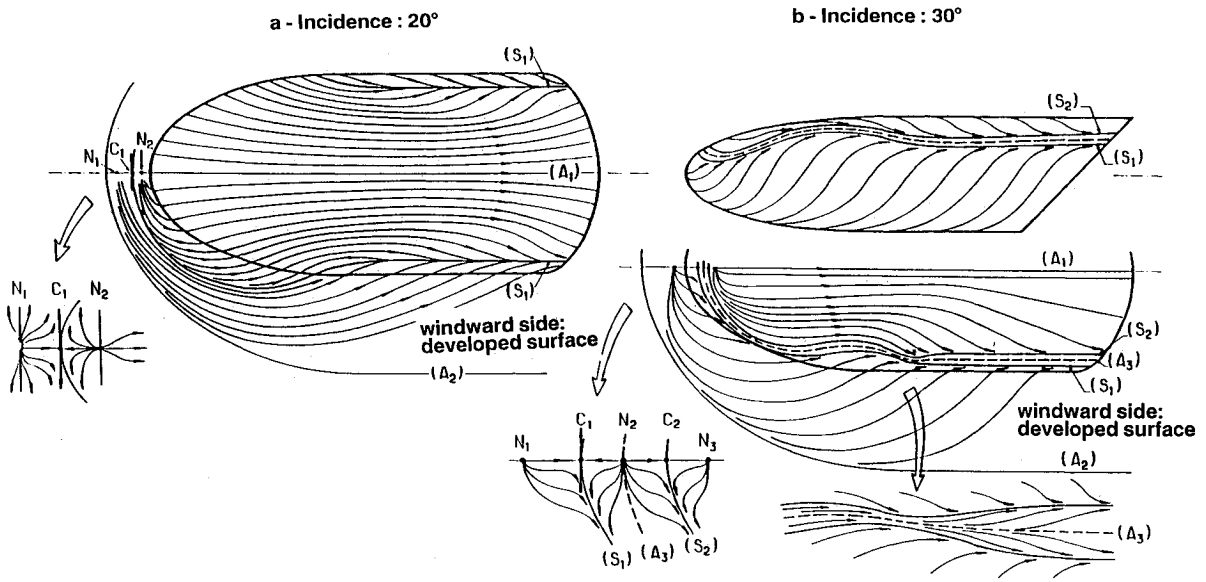

Fig. 32 Blunt-nosed obstacle; topological interpretation of surface flow patterns; upstream velocity V_∞ = 50 m/s.

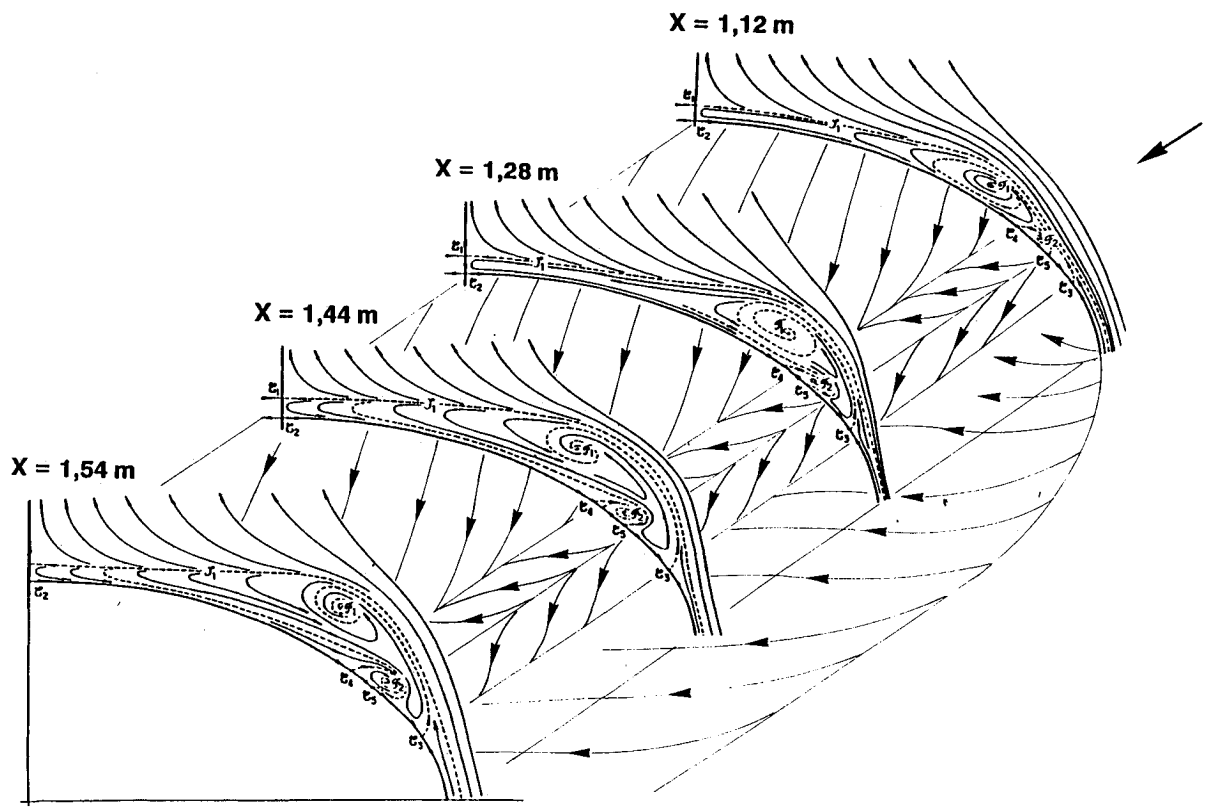

Fig. 33 Blunt-nosed obstacle; topology of the transverse flowfield at an incidence of 30 deg; upstream velocity V_∞ = 50 m/s.

S_1 and the two attachment lines A_1 and A_2, and the second node N_2, which must exist downstream of C_1. Only node N_1 is, in fact, clearly revealed by the visualizations, coinciding with the stagnation point in the usual sense of the term. So N_1 and N_2 are the points of origin of two distinct sets of skin friction lines existing on either side of the separation line S_1.

Similar sketches for $\alpha = 30$ deg are given in Fig. 32b. As previously mentioned, in the present case, two separation lines S_1 and S_2 are clearly visible, especially on the rear part of the model. Also, three attachment lines are present: the two lines A_1 and A_2 that must exist in the vertical plane of symmetry; and line A_3, located between S_1 and S_2. This brings us to introduce the following critical points in the nose region of the model (refer to the enlargement in Fig. 32b): 1) attachment nodes N_1, N_2, and N_3 (N_1 being the stagnation point); and 2) saddle points C_1 and C_2 from which the separation lines S_1 and S_2 originate. It should be noted that only N_1 is clearly revealed by the surface flow visualizations. Also, the existence of C_1 is confirmed by boundary-layer computations.[80]

As in the case of a slender body at low incidence, the separators follow a long path from the point of origin, remaining hardly distinguishable from the neighboring skin friction lines. It is only after the ellipsoid-cylinder junction that these lines begin to deflect rapidly, converging toward the separation lines or diverging from the attachment lines.

In the examination of the vortex organization resulting from separation, we consider the flow configuration obtained for $\alpha = 30$ deg, which has been thoroughly studied by means of surveys using five-hole pressure probes and LDV.

By trajectography in the measured velocity fields and referring to the surface visualizations that show the separation and attachment line positions accurately, the lines of force of the transverse motion can be established (see Fig. 33). The critical points appearing in these plots are 1) the two foci $\mathcal{F}_1$ and $\mathcal{F}_2$; 2) half-saddle points $\mathcal{C}_3$ and $\mathcal{C}_4$, which are the traces of the separation lines S_1 and S_2; 3) half-saddle point $\mathcal{C}_5$ corresponding to attachment line A_3; and 4) saddle point $\mathcal{C}_2$ and half-saddle point $\mathcal{C}_1$ located in the plane of symmetry.

The results obtained on this model for $\alpha = 30$ deg reveal a well-defined organization of the vortex system. Down to an abscissa slightly above 1.12 m, the primary and secondary vortices are contained in a thin layer in contact with the wall, and the dissipative flow structure is then not very different from a classical boundary layer. It is only after $X = 1.12$ m that two vortices effectively "leave" the surface to form a well-organized vortex system associated with clear separation. A clear change in the surface pattern, where the separation and attachment lines become identified corresponds to this evolution.

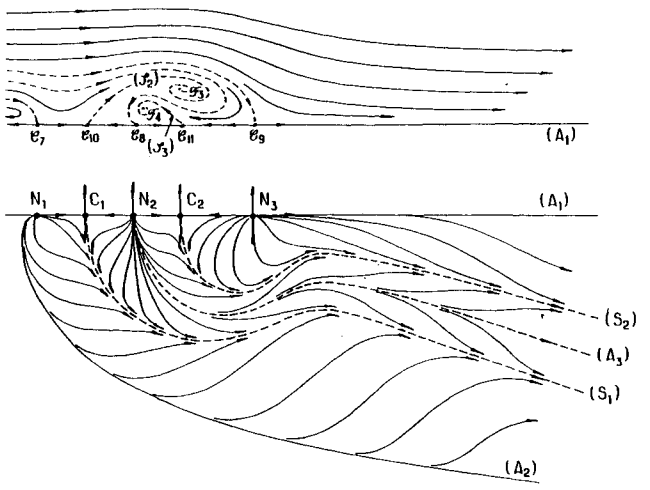

Fig. 34 Blunt-nosed obstacle; flowfield organization; first interpretation.

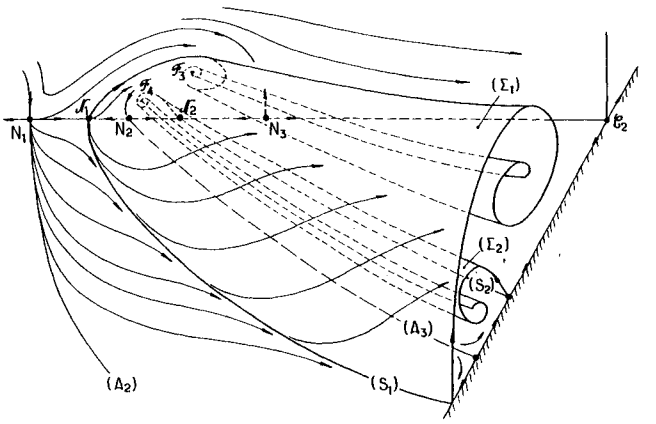

Fig. 35 Blunt-nosed obstacle; separation surfaces; first interpretation.

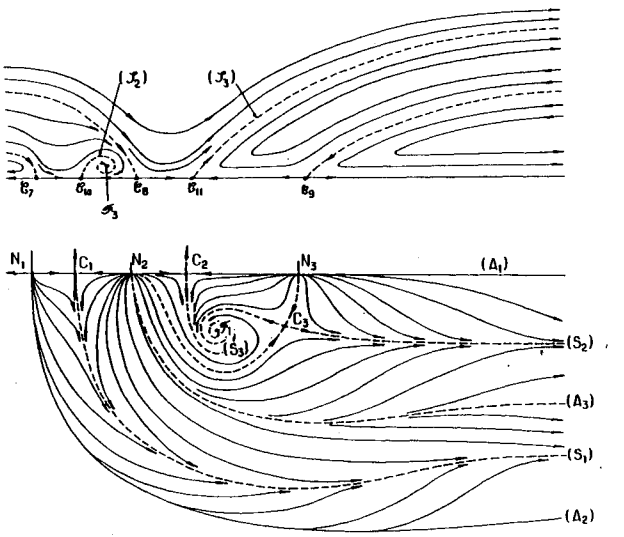

Fig. 36 Blunt-nosed obstacle; flowfield organization; second interpretation.

The schemes we now propose for the flow around the model at an incidence of 30 deg are essentially qualitative, because of the near impossibility of representing things in proportions of reality. As diagrammed in Fig. 34, a plausible configuration can be constructed by introducing five separators and five critical points. To connect this pattern to the outer field in the plane of symmetry, we must associate the three nodes N_1, N_2, and N_3 with the three half-saddle points $\mathcal{C}_7$, $\mathcal{C}_8$, and $\mathcal{C}_9$ through which three separators pass. With saddle points C_1 and C_2 are associated half-saddle points $\mathcal{C}_{10}$ and $\mathcal{C}_{11}$ from which emanate separators $\mathcal{S}_2$ and $\mathcal{S}_3$ winding around foci $\mathcal{F}_3$ and $\mathcal{F}_4$.

The flows on the surface and in the plane of symmetry are the traces of the system consisting of the two horseshoe vortices represented in Fig. 35. A first separation surface Σ_1, whose trace on the surface is the primary separation line S_1, winds around an "axis" passing through focus $\mathcal{F}_3$ in the plane of symmetry. All the streamlines defining Σ_1 originate in node $\mathcal{N}_1$ coincident with half-saddle point $\mathcal{C}_{10}$ in the plane of symmetry and saddle point C_1 on the body surface. In a similar way, a second separation surface (Σ_2) springs from the separation line (S_2), its streamlines coming from node $\mathcal{N}_2$ coincident with $\mathcal{C}_{11}$ and C_2.

Another flow organization may be imagined that is also topologically correct and consistent with the surface visualization and field measurement data (Fig. 36). Let us first consider the surface flow pattern. To the five separators A_1, A_2, A_3, S_1, and S_2, whose existence is proved by the surface flow pattern beyond a need for discussion, we add a third

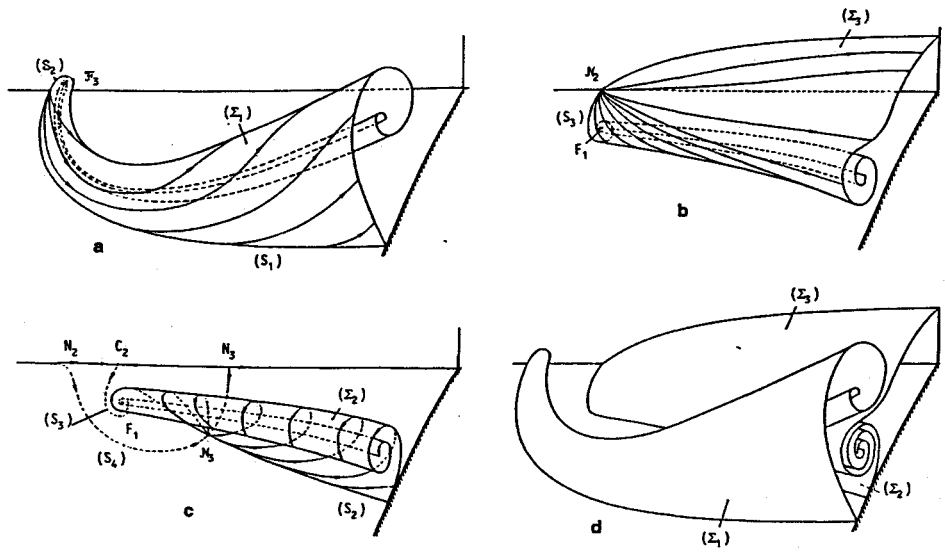

Fig. 37 Blunt-nosed obstacle; separation surfaces; second interpretation.

separation line S_3 coming out of saddle point C_2, which winds around focus F_1. Now, the separation line S_2 also winds around F_1, which is the imprint on the surface of the secondary vortex. For the surface pattern to be consistent, a third saddle point C_3 must exist outside the plane of symmetry, through which separation line S_2 must pass.

The separation surfaces resulting from the present interpretation are drawn in Figs. 37a to 37d. The primary separation surface Σ_1 is first represented in Fig. 37a with its trace on the obstacle being the separation line S_1 and its intersection with the plane of symmetry being the separator $\mathcal{S}_2$, which rolls around the focus $\mathcal{F}_3$. The rolling up of Σ_1 forms a horseshoe vortex. The organization of the second vortex is more complex this time. We first consider (see Fig. 37b) one separation surface Σ_2 whose trace is the separation line S_2, which originates in focus F_1. A second separation surface Σ_3, rolling up inside Σ_2, also originates in F_1 (see Fig. 37c). The set $(\Sigma_2) + (\Sigma_3)$ constitutes a tornado-like vortex. The streamlines defining Σ_2 and Σ_3 start from the half-nodes $\mathcal{N}_3$ and $\mathcal{N}_2$, which, on the model surface, coincide with C_3 and C_2. Figure 37d shows the three surfaces Σ_1, Σ_2, and Σ_3 together forming the primary and secondary vortices.

IV. Conclusion

The critical-point theory is now recognized as being an indispensable basis for any consistent description of a three-dimensional separated flow. In effect, it is a logical tool with a precise terminology for interpreting the results of numerical simulations as well as experimental data. Thus, the critical-point theory allows a precise definition of the skin friction line patterns revealed by surface flow visualizations. Careful decoding of these patterns reveals the presence of the critical points and separators that are signs of the occurrence of separation. The surface patterns are actually the imprints on the obstacle of the outer vortex field and their consideration is a prerequisite to further analysis of the flow.

Explorations by means of multihole pressure probes or three-component LDV systems allow the investigation to extend to the outer field. The combination of surface visualizations and field surveys make possible a detailed and realistic description of vortical flows resulting from separation on obstacles of various shapes. When the obstacle surface has a sharp edge, a separation line is most often coincident with the singularity. This line is the origin of a separation surface, whose rolling up constitutes the primary intense vortex. This circumstance is conducive to modeling of the separated flow in the framework of a perfect fluid approach. However, in this case, secondary vortices also form that are not attached to any singularity of the surface, and whose influence on the field is noticeable.

On a rounded obstacle, whose radius of curvatures is large everywhere compared to the local boundary-layer thickness, no singularity allows the separation line location(s) to be determined a priori. If the body has a sharp nose, experiments tend to show that—even at moderate incidence—the various separators originate in the apex, where the critical points accumulate. As such a degree of singularity is improbable from a physical standpoint, it is likely that the nodes and saddle points where the separators originate are distinct in a small domain near the apex, which is inevitably rounded on a sufficiently small scale.

When the body is blunt, the critical points have no reason to be located in a singular point of the surface. However, for the model considered here, which is close to many practical configurations, these points are all located in the nose region, the "main" attachment node being the only one clearly detected by the visualizations. The oil film technique—whose disturbing effect is not negligible in regions where the thickness of the boundary layer is comparable to that of the film—lacks the fineness required to resolve the real pattern and show the other critical points whose existence is necessary to ensure the topological consistency of the flowfield.

Except at very high incidence, convergence of the skin friction lines toward the separation line(s) occurs only at a certain distance downstream of the model nose or apex. Before, nothing distinguishes a separation line from the other skin friction lines. All along this upstream path, the vortex structures, which necessarily originate in the region of the critical points, are immersed inside the boundary layer and carry a low concentration of vorticity. It is only when convergence of the skin friction lines occurs that these structures leave the surface, carrying away vorticity to form well-identifiable vortices. Then, one can really speak of separation with the usual meaning of the term.

Representation of the very fine phenomena at the origin of the separators requires high computational accuracy with the use of extremely refined meshes. It is probable that such a quality of computation is unnecessary for most applications. Thus, theoretical methods capable of defining the separation lines only when the convergence motion is well characterized are certainly sufficient for predicting "practical" separation, even if the topological consistency of the field is not ensured. The fine structures rubbed out by the lack of refinement of the discretization do not have much influence on the final quality of the results. Of course, the situation may be different for applications in which the scale of these structures is comparable to that of the device, such as in channel flows.

Acknowledgment

This article is an English, condensed version of a paper originally published by the Advisory Group for Aerospace Research and Development of the North Atlantic Treaty Organisation (AGARD/NATO) in a publication entitled "Vortex Flow Aerodynamics," CP 494.

The study of the flow past the ARIANE 5 afterbody was conducted under contract from the Centre National d'Etudes Spatiales (CNES) and the studies of vortex formation past the slender body and the ellipsoid-cylinder with the financial support of the Direction des Recherches, Etudes et Techniques (DRET) and of the Service Technique des Programmes Aéronautiques (STPA) of the French Ministry of Defence. The author is greatly indebted to C. Berner from ISL (French-German Research Institute of Saint-Louis) for having permitted him to present results on the afterbody at an incidence. Last, he is grateful to C. Quélin for the production of most of the figures illustrating this text.

The author expresses his warmest thanks to the reviewer for his suggestions, which greatly helped in clarifying and completing important aspects of three-dimensional flow topology presented in this article.

References

[1]Hitzel, S. M., and Schmidt, W., "Slender Wings with Leading-Edge Vortex Separation: A Challenge for Panel Methods and Euler Solvers," *Journal of Aircraft*, Vol. 21, No. 10, 1984, pp. 751–759.

[2]Rizzi, A. W., and Eriksson, L. E., "Computation of Flow around Wings Based on the Euler Equations," *Journal of Fluid Mechanics*, Vol. 148, 1984, pp. 45–71.

[3]Borrel, M., Montagne, J.-L., Diet, J., Guillen, Ph., and Lordon, J., "Méthode de calcul d'écoulements autour de missiles tactiques à l'aide d'un schéma décentré," (Calculation Method for the Flow past Tactical Missiles with a Non-Centered Scheme), *La Recherche Aérospatiale*, French and English editions, No. 2, 1988, pp. 43–55.

[4]Siclari, M. J., and Del Guidice, P., "Hybrid Finite Volume Approach to Euler Solutions for Supersonic Flows," *AIAA Journal*, Vol. 28, No. 1, 1990, pp. 66–74.

[5]Lordon, J., Fare, J. C., and Pagan, D., "Supersonic Vortex Flows around a Missile Body. Basic Experiment and Euler Numerical Modelisation," AGARD CP 493, 1990.

[6]Kordulla, W., Vollmers, H., and Dallmann, U., "Simulation of Three-Dimensional Transonic Flow with Separation past a Hemisphere-Cylinder Configuration," AGARD CP 412, 1986.

[7]Elsenaar, A., and Eriksson, G., *Proceedings of the Symposium on the International Vortex Flow Experiment on Euler Code Validation*, National Aerospace Lab., The Netherlands, MP-84078U, Stockholm, Sweden, Oct. 1–3, 1986.

[8]Rizzetta, D. P., and Shang, J. S., "Numerical Simulation of Leading Edge Vortex Flows," *AIAA Journal*, Vol. 24, No. 2, 1986, pp. 237–245.

[9]Fuji, K., and Schiff, L. B., "Numerical Simulation of Vortical Flows over a Strake-Delta Wing," *AIAA Journal*, Vol. 27, No. 9, 1989, pp. 1153–1162.

[10]Han, T., "Computational Analysis of Three-Dimensional Turbulent Flow around a Bluff Body in Ground Proximity," *AIAA Journal*, Vol. 27, No. 9, 1989, pp. 1213–1219.

[11]Thomas, J. L., and Newsome, R. W., "Navier-Stokes Computations of Lee-Side Flows over Delta Wings," *AIAA Journal*, Vol. 27, No. 12, 1989, pp. 1673–1679.

[12]Ward, K. C., and Katz, J., "Topology of the Flow Structures Behind an Inclined Projectile: Parts A and B," *Journal of Aircraft*, Vol. 26, No. 11, 1989, pp. 1016–1031.

[13]Chima, R. V., and Yokota, J. W., "Numerical Analysis of Three-Dimensional Viscous Internal Flows," *AIAA Journal*, Vol. 28, No. 5, 1990, pp. 798–806.

[14]Hsu, C. H., and Liu, C. H., "Navier-Stokes Computation of Flow around a Round-Edge Double-Delta Wing," *AIAA Journal*, Vol. 28, No. 6, 1990, pp. 961–970.

[15]Hartwich, P. M., and Hall, R. M., "Navier-Stokes Solutions for Vortical Flows over a Tangent-Ogive Cylinder," *AIAA Journal*, Vol. 28, No. 7, 1990, pp. 1171–1179.

[16]Legendre, R., "Ecoulement au voisinage de la pointe avant d'une aile à forte flèche aux incidences moyennes," (Flow in the Vicinity of the Apex of a Wing with Large Sweep Angle at Moderate Incidences), *La Recherche Aéronautique*, No. 30, 1952, pp. 3–8.

[17]Legendre, R., "Séparation de l'écoulement laminaire tridimensionnel," (Separation of a Laminar Three-Dimensional Flow), *La Recherche Aéronautique*, No. 54, 1956, pp. 3–8.

[18]Legendre, R., "Lignes de courant d'un écoulement permanent. Décollement et séparation" (Streamlines of a Steady Flow. Separation and Separators), *La Recherche Aérospatiale*, No. 6, 1977, pp. 327–335.

[19]Oswatitsch, K., "Die Ablösungsbedingung von Grenzschichten," *Grenzschichtforschung*, edited by H. Görtler, Springer-Verlag, Berlin, 1958, pp. 357–367.

[20]Lighthill, J. M., "Attachment and Separation in Three-Dimensional Flow," *Laminar Boundary-Layer Theory*, edited by L. Rosenhead, Oxford University Press, Oxford, England, UK, Sec. II, Chaps. 2–6, pp. 72–82.

[21]Chanetz, B., "Contribution à l'étude du décollement tridimensionnel en écoulement turbulent incompressible," (Contribution to the Study of Three-Dimensional Separation in Incompressible Turbulent Flow), Ph.D. Dissertation, Univ. Claude Bernard, Lyon, France, Sept. 1986.

[22]Perry, A. E., and Fairlie, B. D., "Critical Points in Flow Patterns," *Advance in Geophysics*, Vol. B-18, 1974, pp. 299–315.

[23]Wang, K. C., "Boundary-Layer over a Blunt Body at Low Incidence with Circumferential Reversed Flow," *Journal of Fluid Mechanics*, Vol. 72, Part I, 1975, pp. 49–65.

[24]Tobak, M., and Peake, D. J., "Topology of Three-Dimensional Separated Flows," *Annual Review of Fluid Mechanics*, Vol. 14, 1982, pp. 61–85.

[25]Dallmann, U., "Topological Structures of Three-Dimensional Flow Separation," DFVLR-IB 221–82, 1983.

[26]Hornung, H., and Perry, A. E., "Some Aspects of Three-Dimensional Separation. Part I: Streamsurface Bifurcations," *Zeitschrift für Flugwiss. Weltraumforsch.* 8, Heft, 2, 1984, pp. 77–87.

[27]Perry, A. E., and Chong, M. S., "A Description of Eddying Motions and Flow Patterns Using Critical Point Concepts," *Annual Review of Fluid Mechanics*, Vol. 19, 1987, pp. 125–155.

[28]Kaynak, U., Cantwell, B. J., Holst, T. L., and Sorensen, R. L., "Numerical Simulation of Transonic Separated Flows over Low Aspect Ratio Wings," AIAA Paper 86-0508, Reno, NV, Jan. 1986.

[29]Mehta, R. D., and Lim, T. T., "Flow Visualization Study of a Vortex/Wing Interaction," NASA TM-86 656, 1986.

[30]Doerffer, P., and Dallmann, U., "Reynolds Number Effect on Separation Structures at Normal Shock Wave/Turbulent Boundary Layer Interaction," *AIAA Journal*, Vol. 27, No. 9, 1989, pp. 1206–1212.

[31]Doerffer, P., and Dallmann, U., "Mach Number Dependence of Flow Separation-Induced by Normal Shock Wave/Turbulent Boundary Layer Interaction at a Curved Wall," AIAA Paper 89-0353, Reno, NV, Jan. 1989.

[32]Legendre, R., "Evolution régulière ou catastrophique d'écoulements permanents dépendant de paramètres," *La Recherche Aérospatiale*, No. 4, 1982, pp. 225–232.

[33]Chapman, G. T., "Topological Classification of Flow Separation on Three-Dimensional Bodies," AIAA Paper 86-0485, Reno, NV, Jan. 1986.

[34]Hornung, H., "The Vortex Skeleton Model for Three-Dimensional Steady Flows," AGARD CP 342, 1983.

[35]Perry, A. E., and Hornung, H., "Some Aspects of Three-Dimensional Separation. Part II: Vortex Skeleton," *Zeitschrift für Flugwiss. Weltraumforsch.* 8, Heft 3, 1984, pp. 155–160.

[36]Maskell, E. C., "Flow Separation in Three Dimensions," Royal Aircraft Establishment Aero Rept. 2565, Nov. 1955.

[37]Visbal, M., "Numerical Investigation of Laminar Juncture Flow," AIAA Paper 89-1873, Reno, NV, 1989.

[38]Hung, C. M., Sung, C. H., and Chen, C. L., "Computation of Saddle Point of Attachment," AIAA Paper 91-1713, June 1991.

[39]Ginoux, J., "Experimental Evidence of Three-Dimensional Perturbations in the Reattachment of a Two-Dimensional Laminar Boundary Layer," Von Kàrmàn Inst., TN-1, 1958.

[40]Settles, G. S., Fitzpatrick, T. J., and Bogdonoff, S. M., "A Detailed Study of Attached and Separated Compression Corner Flowfields in High Reynolds Number Supersonic Flow," *AIAA Journal*, Vol. 17, No. 6, 1979, pp. 579–585.

[41]Roshko, A., and Thomke, G. J., "Observations of Turbulent Reattachment behind an Axisymmetric Downstream Facing Step in Supersonic Flow," *AIAA Journal*, Vol. 4, No. 6, 1966, pp. 975–980.

[42]Joulot, A., private communication, 1990.

[43]Inger, G. R., "Three-Dimensional Heat and Mass Transfer Effects across High-Speed Reattaching Flows," *AIAA Journal*, Vol. 15, No. 3, 1977, pp. 383–389.

[44]Peake, D. J., and Tobak, M., "Three-Dimensional Interactions and Vortical Flows with Emphasis on High Speed," AGARDograph

252, March 1980.

[45]Werlé, H., "Ecoulements décollés. Etude phénoménologique à partir de visualisations hydrodynamiques," (Separated Flows. A Phenomenological Study From Visualizations in a Water Tunnel), ONERA TP 1975-14, 1975.

[46]Cambier, L., and Escande, B., "Navier-Stokes Simulation of a Shock Wave/Turbulent Boundary Layer Interaction in a Three-Dimensional Channel." AIAA Paper 89-1851, Buffalo, New York, June 1989; see also, *AIAA Journal*, Vol. 28, No. 11, 1990, pp. 1901–1908.

[47]Benay, R., Délery, J., and Pot, T., "Analyse expérimentale de l'écoulement dans un canal transsonique tridimensionnel" (Experimental Analysis of the Flow in a Three-Dimensional Transonic Channel), *La Recherche Aérospatiale*, French and English editions, No. 6, 1986, pp. 399–414.

[48]Green, J. E., "Interactions Between Shock Waves and Turbulent Boundary Layers," *Progress in Aerospace Sciences*, edited by D. Küchemann et al., Vol. II, Pergamon, Oxford, 1970.

[49]Reda, D. C., and Murthy, J. D., "Shock Wave/Turbulent Boundary Layer Interactions in Rectangular Channels," AIAA Paper 72-715, Boston, MA, 1972; see also, *AIAA Journal*, Vol 11, No. 2, 1973, pp. 139–140.

[50]Schofield, W. H., "Turbulent Boundary Layer Development in an Adverse Pressure Gradient after an Interaction with a Normal Shock Wave," *Journal of Fluid Mechanics*, Vol. 154, 1985, pp. 43–62.

[51]Dallmann, U., and Schewe, G. "On Topological Changes of Separating Flow Structures at Transition Reynolds Numbers," AIAA Paper 87-1266, Honolulu, HI, June 1987.

[52]Reijasse, Ph., and Délery, J., "Analyse expérimentale de l'écoulement au culot de l'arrière-corps du lanceur ARIANE 5. Exploitation des résultats" (Experimental Analysis of the Flow at the Base of the ARIANE 5 Afterbody. Exploitation of the Results), ONERA Rept. 6/4362AY, Nov. 1989.

[53]Hummel, D., "On Vortex Formation over a Slender Wing at Large Angles of Incidence," AGARD CP 247, Jan. 1976.

[54]Hoeijmakers, H. W. M., Vaatstra, W., and Verhaagen, N. G., "Vortex Flow over Delta and Double-Delta Wings," *Journal of Aircraft*, Vol. 20, No. 9, 1983, pp. 825–832.

[55]Taylor, S. L., Kjelgaard, S. O., Weston, R. P., Thomas, J. L., and Sellers III, W. L., "Experimental and Computational Study of the Subsonic Flow about a 75° Swept Delta-Wing," AIAA Paper 87-2425, Aug. 1987.

[56]Elsenaar, A., and Bütefisch, K. A., "Experimental Study on Vortex and Shock Wave Development on a 65° Delta Wing," *Symposium Transsonicum III*, edited by J. Zierep and H. Oertels, Springer-Verlag, Berlin, 1988.

[57]Narayan, K. Y., and Hartmann, K., "Transonic and Supersonic Flow past a 65° Delta Wing with Rounded Leading Edges. Analysis of Experimental Data," DFVLR FB 88-44, 1988.

[58]Kegelman, J. T., and Roos, F. W., "The Flowfields of Bursting Vortices Over Moderately Swept Delta Wings," AIAA Paper 90-0599, Reno, NV, Jan. 1990.

[59]Pagan, D., and Solignac, J.-L., Etude expérimentale de la formation des nappes tourbillonnaires sur une aile delta en écoulement incompressible" (Experimental Study of Vortex Sheet Formation on a Delta Wing in Incompressible Flow), ONERA Rept. 34/1147 AY, April 1985.

[60]Molton, P., "Aile delta en écoulement incompressible. Etude expérimentale à F2" (Delta Wing in an Incompressible Flow. Experimental Study in the F2 Wind Tunnel), ONERA Rept. 36/1147 AN, Dec. 1986.

[61]Solignac, J.-L., Pagan, D., and Molton, P., "Etude expérimentale de l'écoulement à l'extrados d'une aile delta en régime incompressible" (Experimental Study of the Flow on the Suction Side of a Delta Wing in Incompressible Flow), *La Recherche Aérospatiale*, French and English editions, No. 6, 1989, pp. 47–65.

[62]Monnerie, B., and Werlé, H., "Etude de l'écoulement supersonique et hypersonique autour d'une aile élancée en flèche" (Study of the Supersonic and Hypersonic Flow Past a Slender, Highly Swept Wing), AGARD CP 30, 1968.

[63]Délery, J., and Lacau, R. G., "Prediction of Base-Flows," *Special Course on Missile Aerodynamics*, AGARD Rept. 754.

[64]Berner, C., "Measurements and Interpretation of 3-D High Speed Flows," *Proceedings of the Third International Conference on Laser Anemometry*, Swansea, Wales, UK, Sept. 26–29, 1989 and French-German Inst. of Saint-Louis, Rept. CO 242/89.

[65]Berner, C., and Dupéroux, J. P., "Mesures simultanées des trois composantes du vecteur vitesse dans le sillage d'arrière-corps à symétrie de révolution et en incidence" (Simultaneous Measurements of the Velocity Vector Three Components in the Wake of an Axisymmetric Afterbody at an Incidence), French-German Inst. of Saint-Louis, Rept. S-CR 2/90, 1990.

[66]Jorgensen, L. H., and Perkins, E. W., "Investigation of Some Wake Vortex Characteristics of an Inclined Ogive-Cylinder Body at Mach Number 1.98," NACA RM-A55E31, Aug. 1955.

[67]Fidler, J. E., Schwind, R. G., and Nielsen, J. N., "Investigation of Slender-Body Vortices," *AIAA Journal*, Vol. 15, No. 12, Dec. 1977, pp. 1736–1741.

[68]Yanta, W. J., and Wardlaw, A. B., Jr., "Flowfield about and Forces on Slender Bodies at High Angles of Attack," *AIAA Journal*, Vol. 19, No. 3, 1981, pp. 296–302.

[69]Yanta, W. J., and Wardlaw, A. B., Jr., "The Secondary Separation Region on a Body at High Angles of Attack," AIAA Paper 82-0343, Orlando, FL, Jan. 1982.

[70]Ponton, A. J. C., and Johnson, G. A., "The Analysis and Modelling of Body Vortex Flowfields around Missile Configurations and their Interaction with Lifting Surfaces at Subsonic and Supersonic Speeds," *The Prediction and Exploitation of Separated Flows*, Royal Aeronautical Society, Paper 26, 1989.

[71]Champigny, P., and Baudin, D., "Ecoulement tourbillonnaire sur fuselage de missile. Etude expérimentale et modélisation" (Vortical Flow on the Fuselage of a Missile. Experimental Study and Modeling), AGARD CP 494, 1991.

[72]Pagan, D., and Molton, P., "Etude expérimentale du système tourbillonnaire engendré par un fuselage de missile en incidence. Première partie: couche limite laminaire" (Experimental Study of the Vortex System Generated by a Missile Fuselage at an Angle of Incidence. First Part: Laminar Boundary Layer), ONERA Rept. 40/1147AY, Jan. 1990.

[73]Eichelbrenner, E. A., and Oudard, A., "Méthode de calcul de la couche limite tridimensionnelle" (Calculation Method for the Three-Dimensional Boundary Layer), ONERA Publication 76, 1955.

[74]Vollmers, H., Kreplin, H. P., and Meier, H. U., "Separation and Vortical-Type Flow Around a Prolate Spheroid. Evaluation of Relevant Parameters," AGARD CP-342, 1983.

[75]Meier, H. U., Kreplin, H. P., Landhauber, A., and Baumgarten, D., "Mean Velocity Distribution in Three-Dimensional-Boundary Layers Developing on a 1:6 Prolate Spheroid with Artificial Transition," DFVLR-IB 222-24-A11, 1984.

[76]Costis, C. E., Polen, D. M., Hoang, N. T., and Telionis, D. P., "Laminar Separating Flow over a Prolate Spheroid," AIAA Paper 87-1212, Honolulu, HI, June 1987.

[77]Hoang, N. T., Telionis, D. T., and Jones, G. S., "The Hemisphere-Cylinder at an Angle of Attack," AIAA Paper 90-0050, Reno, NV, Jan. 1990.

[78]Werlé, H., "Principaux types de décollements libres observés sur maquettes ellipsoïdales" (Main Types of Free Separation Observed on Ellipsoid Type Models), ONERA TN 1985–7, 1985.

[79]Chanetz, B., and Délery, J., "Etude expérimentale du décollement turbulent sur un ellipsoïde-cylindre aplati" (Experimental Analysis of Turbulent Separation on an Oblate Ellipsoid-Cylinder), *La Recherche Aérospatiale*, French and English editions, No. 3, 1988, pp. 59–77.

[80]Barberis, D., "Calcul de la couche limite tridimensionnelle en modes direct ou inverse sur des obstacles quelcónques" (Direct Mode and Inverse Mode Calculations of the Three-Dimensional Boundary Layer past Arbitrary Bodies), *La Recherche Aérospatiale*, French and English editions, No. 3, 1986.